Cell Communication and Signaling

https://doi.org/10.1186/s12964-025-02635-9

Article in Press

A pro-carcinogenic oral microbe internalized by breast cancer cells promotes mammary tumorigenesis

Received: 15 October 2025

Accepted: 26 December 2025

Published online: 15 January 2026

Cite this article as: Parida S., Nandi D., Verma D. *et al.* A pro-carcinogenic oral microbe internalized by breast cancer cells promotes mammary tumorigenesis. *Cell Commun Signal* (2025). https://doi.org/10.1186/s12964-025-02635-9

Sheetal Parida, Deeptashree Nandi, Deepak Verma, Mingyang Yi, Ashutosh Yende, Jessica Queen, Kathleen L. Gabrielson, Cynthia L. Sears & Dipali Sharma

A pro-carcinogenic oral microbe internalized by breast cancer cells promotes mammary tumorigenesis

Sheetal Parida[1], Deeptashree Nandi[1], Deepak Verma[1], Mingyang Yi[1], Ashutosh Yende[1], Jessica Queen[1], Kathleen L. Gabrielson[1,2], Cynthia L. Sears[1,3], and Dipali Sharma[1]

[1]Department of Oncology, Sidney Kimmel Comprehensive Cancer Center, Johns Hopkins University School of Medicine, Baltimore, Maryland, USA; [2]Department of Molecular and Comparative Pathobiology, Johns Hopkins University School of Medicine, Baltimore, Maryland, USA; [3]Bloomberg-Kimmel Institute for Cancer Immunotherapy, Johns Hopkins University School of Medicine, Baltimore, Maryland, USA

Running title: *F. nucleatum* promotes breast carcinogenesis

Key words: oral dysbiosis, breast cancer, *F. nucleatum*, BRCA mutant cells, DNA damage

* **Corresponding author:**

Dipali Sharma, Department of Oncology

The Sidney Kimmel Comprehensive Cancer Center,

Johns Hopkins University School of Medicine,

1650 Orleans Street, CRB 1, Rm 145, Baltimore, MD 21231

Office: 410-455-1345, FAX: 410-614-4073,

Email: dsharma7@jhmi.edu

Total number of figures: 7

Conflict of Interest: The authors declare no conflict of interest.

Abstract

The intricate relationship between microbiota and breast cancer presents an additional risk factor that can have a profound impact on disease progression. Focusing on dysbiosis, our metagenomic analysis shows overabundance of an oral pathogenic microbe *F. nucleatum* and co-habitation of associated biofilm forming oral microbes in cancerous breast. Mammary gland colonization with *F. nucleatum* results in the development of metaplastic lesions accompanied with inflammation, DNA damage and hyper-proliferation in healthy mice. Exhibiting the impact of circulating *F. nucleatum* introduced via hematogenous route, breast tumor bearing mice show accelerated tumor growth and metastatic progression. Increased proliferation, migration, self-renewal and chemoresistance in breast cancer cells as well as non-tumorigenic breast epithelial cells bearing pathogenic BRCA1 mutation is observed upon *F. nucleatum* exposure which is internalized by the cells in a Gal-GalNAc dependent manner. Of interest, cells harboring BRCA1 mutations exhibit greater cell surface accumulation of Gal-GalNAc sugar residue. This work sheds light on the oncogenic impact of a pro-carcinogenic oral bacterium, *F. nucleatum*, on normal mammary epithelium and breast cancer, implicates the impairment of DNA damage and repair pathways as its functional mediators, and proposes the concept of increased vulnerability of BRCA1 mutant breast cancer cells owing to their preferential internalization of *F. nucleatum*.

Significance: Oral microbe *F. nucleatum* also inhabits breast cancer tissue, and mammary duct colonization or hematogenous administration with pathogenic *F. nucleatum* triggers metaplastic lesions and augments breast cancer growth and metastasis. BRCA1 mutant breast epithelial cells exhibit susceptibility to *F. nucleatum* internalization, retention and ensuing biological implications.

Introduction

In the US, 1 in 8 women encounter a lifetime risk of developing breast cancer, and it remains a leading cause of morbidity and mortality among women globally. Traditionally known risk factors for breast cancer include gender, age, environmental exposures to toxins, alcohol and tobacco use, high breast density, premalignant disease, personal history of cancer and obesity. A strong genetic predisposition to breast cancer has also been identified; about 15% of women diagnosed with breast cancers have a family history of cancer. Women with first degree relative diagnosed with breast cancer face twice the likelihood, and women having two first degree relatives with breast cancer have thrice the probability of developing it in their lifetime [1, 2]. Approximately, 5-10% of total breast cancers can be attributed to germline mutations in BRCA1/2, CDH1, TP53, PTEN, CHEK2, BRIP1, PABL2 and ATM. Among these, BRCA1 mutations are the most frequently detected aberrations in familial breast cancers. However, 30-45% of women with inherited BRCA1 mutations do not develop breast cancers (https://www.cancer.org/cancer/types/breast-cancer/risk-and-prevention/breast-cancer-risk-factors-you-cannot-change.html). Clearly, cumulative effect of genetic disposition and environmental or lifestyle factors drive breast cancer initiation. Recent research has highlighted the critical role of the human microbiota in modulating cancer development and progression[3]. Breast tumors harbor a distinct population of microbiota in comparison to paired normal breast tissue, and malignant tumors exhibit prevalence of certain pathogenic bacteria [4-7]. Diversity observed in the breast tissue microbiota composition [8, 9] indicates that breast microbial dysbiosis may play an important role in breast cancer growth as well as metastatic progression. Gut microbiota may also influence breast cancer as fecal microbiota in postmenopausal women with breast cancer is compositionally different from healthy volunteers [10] exhibiting abundance of several bacterial species [11]. We have previously shown that gut as well as local mammary gland microbiota modulation leads to the development of hyperplastic mammary lesions in wildtype mice [12] as well as alterations in tumor microenvironment and metastatic sites to aid metastatic progression [13].

In addition to gut and breast, the oral cavity hosts a complex ecosystem of microbial diversity and *F. nucleatum* is a well-established constituent of the oral microbiota that plays a significant role in the pathogenesis

of periodontal disease[14]. Interestingly, epidemiological studies have indicated a correlation between periodontal disease with multiple cancers including breast cancer incidence [15-19] thereby indirectly connecting *F. nucleatum* abundance with carcinogenesis. Direct impact of *F. nucleatum* abundance has been mostly shown in colorectal cancer and several mechanistic insights have been reported. *F. nucleatum* promotes colorectal carcinogenesis via multiple mechanisms including E cadherin/Wnt/β-catenin [20], microRNA-31 [21], microRNA-4717-3p [22] and TLR4/NFκB pathways modulating the tumor microenvironment and imparting resistance to chemotherapy and immunotherapy [23-25]. Also, *F. nucleatum* mediated mechanisms leading to increased incidence, aggressiveness and therapy resistance have been proposed in pancreatic cancer [26, 27], oral cancer [28-34] and head and neck cancers [35-41] although data are not uniform. In multiple cancer tissue samples, *F. nucleatum* has been detected via metagenomic analyses. While the route of *F. nucleatum* colonization in the breast remains to be determined, it is thought to translocate through the mammary-intestinal axis, direct nipple contact, and/or hematogenous transmission [42]. In mouse models of breast cancers, *F. nucleatum* has been shown to alter tumor immune-environment [43], promote PD-L1 expression in cancer cells to evade $CD8^+$ T cell killing [44] and modulate TLR4 signaling in breast cancer [45]. Indeed, *F. nucleatum* is now considered an important oral microbe capable of direct pro-oncogenic actions in several organs.

We identified the presence of *F. nucleatum* in benign and malignant breast tumors forming the rationale of our hypothesis that *F. nucleatum* exposure may lead to growth and progression of breast cancer. Consequently, we aim to decipher i) whether intraductal exposure to *F. nucleatum* impacts normal mammary epithelial tissue, ii) whether hematogenous exposure of *F. nucleatum* can promote growth and metastatic progression of existing breast tumors, iii) examine the underlying mechanistic networks and cellular uptake of *F. nucleatum*. Our results demonstrate that intraductal colonization with *F. nucleatum* leads to the formation of metaplastic lesions in mammary glands of healthy mice. *F. nucleatum* exposure increases breast cancer growth and metastatic progression to lungs when administered via hematogenous route. Mechanistically, *F. nucleatum* induces DNA damage and activates the non-homologous end joining (NHEJ) pathway via upregulation of DNA-dependent protein kinase catalytic subunit (DNA-PKcs), and promotes invasion, migration and stemness of breast cancer

cells. Most importantly, BRCA1-mutant breast cells exhibit elevated levels of Gal-GalNAc sugar residue, and cellular uptake and retention *F. nucleatum* is proportional to the level of cell surface accumulation of Gal-GalNAc sugar residue in breast cells indicating that *F. nucleatum* exposure may selectively promote BRCA1-mutnat cells to a greater extent.

Results

Intraductal colonization with *F. nucleatum* leads to the formation of metaplastic lesions in mammary glands of healthy mice. Analyzing multiple datasets examining the breast tumors and gut microbiota of breast cancer patients, and correlating them to the clinicopathological information, we observed that a considerable proportion of breast tumors harbored opportunistic oral pathogens. We particularly focused on bioproject PRJNA335375 [46] as this dataset comprised of 16S rRNA sequencing data from buccal swab, skin swab, skin tissue and breast tissue from breast cancer patients as well as multiple negative controls. We detected an overabundance of biofilm-forming oral microbes, *Fusobacterium nucleatum*, *Veillonella atypica*, *Veillonella dispar* and *Veillonella parvula* in the breast tissue samples from women with benign and malignant breast disease. Interestingly, the abundance of these bacteria in breast tumors positively correlated with the oral levels of these opportunistic pathogens in the same patient (Fig. 1a). Moreover, such correlation was not observed in tissue samples from other body sites (Fig. 1a). Since periodontal disease correlates with multiple cancers including breast cancer [15-17], oral pathogens may exert direct/indirect pro-cancer effects at distant sites. Among these oral microbes unexpectedly accumulated in breast cancer tissue, *F. nucleatum* is a common member of the oral microbiota as well as an opportunistic periodontal pathogen in some individuals; *F. nucleatum* has been known to modulate several oncogenic molecular mechanisms leading to increased incidence, aggressiveness and therapy resistance in multiple cancer types including pancreatic, oral and head & neck cancers [26-41]. *F. nucleatum* also induces a proinflammatory tumor microenvironment and causes metabolic alterations in colorectal cancer [47, 48]. Together, identification of *F. nucleatum* in malignant breast tissue combined with our understanding of the pathogenic role of *F. nucleatum* in several cancers led us to hypothesize that *F. nucleatum* may contribute to breast pathogenesis in healthy mice.

To examine the impact of *F. nucleatum* colonization on normal mammary ductal tissue, we intraductally colonized the mammary ducts of healthy wild type BALB/c and immunodeficient NOD-SCID-gamma (NSG) mice with two strains of *F. nucleatum*; ATCC23726, procured from ATCC and Fn146CP, isolated from the tumor of a colorectal carcinoma patient (Fig. 1b). On colonizing the mammary ducts with either of the strains of *F.*

nucleatum, we observed metaplastic lesions in the mammary tissue accompanied with inflammation, DNA damage and hyper-proliferation (Fig. 1c-f, Supplementary Fig. 1). Upon closer pathological examination of the mammary tissue, we discovered that the mammary gland of *F. nucleatum* FN27236 and FN146CP groups developed more severe lesions while sham-control NSG mice presented some age-related hyperplastic lesions (Fig. 1c). Next, we scored the lesions using several pathologically important criteria to develop a 'severity index' (Supplementary 1a). In NSG mice, the lesions developed in sham-control group resembled squamous cell metaplasia, and were characterized by inflammation, presence of some giant multinucleated cells, granulated mast cells, macrophages and neutrophils, as well as lipofuscin and collagen accumulation. In contrast, the metaplastic and hyperplastic lesions observed in the mammary ducts of NSG mice harboring FN27236 and FN146CP were more abundant as well as more severe. Significantly higher degree of inflammation and fibrosis characterized by collagen accumulation around the ducts was distinctly noted. Higher population of multi-nucleated giant cells was also observed. A significantly higher abundance of mast cells, macrophages and neutrophils was evident. Most importantly, the lesions were clearly more proliferative (Fig. 1d, e). On the other hand, in wild-type BALB/c mice, the sham-control group did not possess any mammary epithelial lesions. The mammary tissue of BALB/c mice harboring FN27236 or FN146CP displayed the presence of metaplastic lesions, and were severely inflamed, marked by the presence of plasma cells, neutrophils, macrophages, lymphocytes, B cells and T cells. Additional features including predominantly granular macrophages and abnormally large lymph nodes with prominent germinal centers, as well as areas of abscess, fat necrosis, tubular necrosis, cytogranuloma and sinus histiocytosis were commonly noted in FN27236 or FN146CP group. Ducts and lymph nodes have multiple layers suggesting hyper-proliferative nature. Most tissue sections showed multiple epithelial layers that were hyper-proliferative. Extensive collagen accumulation around the ducts suggested increased fibrosis (Fig. 1d, f). Importantly, the severity of the lesions observed in sham mice was significantly lower compared to the *F. nucleatum* harboring mice. In NSG mice, sham-control scored 1.4±0.6519 while FN-inoculated mice scored 2.425±0.9432 and 2.5±1.414 for FN27236 and FN146CP respectively, on severity index. Similarly, in wild-type BALB/c mice, sham mice scored 0.75±0.2739 and infected mice scored 4.438±0.9797 and 3.625±0.9161 for FN27236 and

FN146CP respectively (Figure 1d). Not only did we observe a greater number of lesions in the mammary tissue of *F. nucleatum* harboring mice, the size of lesions was also larger. In NSG sham-control mice, 87.5% of mammary lesions were smaller than 20,000 μm^2 and only 12.5% of mammary lesions were larger than 40,000 μm^2 in size. While in NSG mice harboring FN27326, 64.7% of the lesions were smaller than 20,000 μm^2, 7.4% lesions were between 20,000-40,000 μm^2 and 27.9% of the lesions were larger than 40,000 μm^2 in size. In FN146CP harboring NSG mice, 42.57% of the lesions were smaller than 20,000 μm^2, 11.8% lesions were between 20,000-40,000 μm^2 and 45.5% of the lesions were larger than 40,000 μm^2 in size (Figure 1e). In wild-type BALB/c sham-control group, most of the lesions (73.68 %) were smaller than 50,000 μm^2, and only 26.3% lesions were larger than 100,000 μm^2 in size. While in FN27326 harboring BALB/c mice, 58% of the lesions were smaller than 50,000 μm^2, 16% lesions were between 50,000-100,000 μm^2 and 28% of the lesions were larger than 100,000 μm^2. In FN146CP group, 60% of the lesions were smaller than 50,000 μm^2, 20% lesions were between 50,000-100,000 μm^2 and 20% of the lesions were larger than 100,000 μm^2 (Figure 1f). Together, these data indicate the presence of *F. nucleatum* in human breast cancer tissue and show that intraductal exposure to *F. nucleatum* FN27236 and FN146CP is sufficient to exert pathogenic effects on otherwise healthy mammary gland.

***F. nucleatum* exposure increases breast cancer growth and metastatic progression to lungs when administered via hematogenous route.** Oral microbial dysbiosis is known to impact the host beyond oral cavity at a systemic level [49]. While the exact mechanism of tumor specific accumulation of oral microbes at distant sites is poorly understood, they are speculated to translocate from the oral cavity via hematogenous route to different locations. To understand the effect of *F. nucleatum* exposure on the progression of breast tumors, independent of systemic adaptive response to the bacterium, we utilized an orthotopic breast cancer model by inoculating 4×10^6 HCC1806 triple negative breast cancer cells in the mammary glands of NSG mice. Once tumors were palpable, 1×10^8 CFUs of FN27236 or FN146CP were inoculated via tail vein injection, and tumor progression was monitored for 6 weeks. Intravenous *F. nucleatum* inoculation significantly accelerated the growth of HCC1806-derived tumors without any signs of systemic toxicity. Tumors developed in FN27236 or FN146CP

group exhibited significantly increased tumor volume and weight compared to sham-control group (Fig. 2a, b). While there was no significant difference in the weights of liver, lungs and heart among mice from different experimental groups (Fig. 2c), the spleens of the mice from FN27236 or FN146CP groups were significantly enlarged. Histological analysis of the tumor sections showed an increased stromal infiltration in *FN27236* or *FN146CP* groups along with a significantly higher number of Ki67-positive nuclei in comparison to sham-control mice (Fig. 2d). Most importantly, 100% of the *FN27236* or *FN146CP*-exposed mice developed wide-spread metastasis in the lungs as opposed to only 20% mice in the sham-control group (Fig 2e, f). To understand the sustained impact of hematogenous dissemination of *F. nucleatum* on tumor cells growing in mammary glands of mice, tumors were dissociated into single cells and assessed for their functional potential pertaining to motility and stem-like characteristics. Tumor-dissociated cells from HCC1806-derived tumors developed in mice exposed to *FN27236* or *FN146CP* were significantly more motile and stem-like compared to the sham-control tumors-derived cells as evidenced by accelerated wound-healing response (Fig. 3a) and mammospheres formation (Fig. 3b) and expression of self-renewal markers, Oct4 and Nanog (Fig. 3c, Supplementary Figure 2a). Also, tumor-dissociated cells from HCC1806-derived tumors developed in mice exposed to *FN27236* or *FN146CP* were more proliferative as revealed with PCNA expression (Fig. 3c, Supplementary Figure 2a). To further elucidate the molecular basis of these functional implications, tumors developed in sham-control and *F. nucleatum*-administered mice were subjected to RNA-sequencing (RNA-seq) analysis. A differential expression analysis, conducted to characterize the global differences in RNA transcript levels altered with *F. nucleatum* exposure exhibited 16,214 differentially expressed genes (DEGs) across two distinct groups. Heatmap showed the unsupervised gene clustering of DEGs which confirmed separate clusters for sham-control and *F. nucleatum* group (Supplementary Fig. 2b-d). Next, we analyzed the DEGs between sham and *F. nucleatum* group which showed a total of 1,357 DEGs (p value ≤ 0.05) differentially upregulated or downregulated among the *F. nucleatum* group compared to sham-controls. While 221 genes showed a differential reduction of more than 2-fold (p value ≤ 0.05) in *F. nucleatum* group, only 27 genes exhibited a differential increase of more than 2-fold (p value ≤ 0.05) in *F. nucleatum* group compared to sham control (Fig. 3d). Gene set enrichment analysis (GSEA)

uncovered the enrichment of several important Oncogene and Hallmark Gene signatures including EMT, mTORC, Myc, KRas, Wnt, βcatenin pathways among others (Fig. 3e, Supplementary Fig. 3a-d). Additionally, RNA-seq data obtained from the *F. nucleatum* exposed tumors showed higher expression of genes associated with metastatic progression in comparison to tumors developed in sham-control mice (Fig. 3f, Supplementary Fig. 3e-f). These results suggest that hematogenous administration of *F. nucleatum* accelerates growth of pre-existing breast tumors, causes distinct changes at the gene expression level, and imparts elevated migration and stemness potential to tumor cells supporting higher lung metastasis.

***F. nucleatum* induces DNA damage and activates the NHEJ pathway via upregulation of DNA-PKcs.** It has been known that DNA damage contributes to cancer initiation and progression [50], and DNA damage response and repair can be modulated by pathogenic bacteria [51-53]. *F. nucleatum* causes DNA damage in oral cancer [33], colorectal cancer [54], esophageal squamous cell carcinoma [55] and squamous cell carcinoma of the head and neck [36]. To query the underlying pathways associated with *F. nucleatum* exposure in human breast cancer cell-derived tumors, we further analyzed the RNA-seq data obtained from the tumors developed in *F. nucleatum*-administered or sham-control mice. GSEA showed the enrichment of DNA damage and repair pathway gene signatures (Fig. 4a). Additionally, RNA-seq data obtained from the *F. nucleatum* exposed tumors showed higher expression of genes associated with DNA damage and repair pathway in comparison to tumors developed in sham-control mice (Fig. 4b, Supplementary Figure 4). To garner further support, we analyzed the bulk RNA sequencing data set, GSE144143, comparing the gene expression of murine breast epithelial cell line, AT3 to AT3 cells co-cultured with *FN27236* for 24 hours. The raw sequencing reads were downloaded from NCBI-SRA and re-analyzed using DEseq2 pipeline followed by gene set enrichment analysis (GSEA). Among the multiple genes and pathways enriched in AT3-*FN27236* co-cultured cells, fatty acid metabolism, E2F targets, apical surface, adipogenesis and DNA repair, were the top five, statistically significant, upregulated pathways (Supplementary Fig 5a-c). DNA damage response (DDR) pathway is generally initiated with a double-stranded break (DSB) in the genome of mammalian cells activating the DSB sensors. Serving as a substrate for these DSB

sensors, γ-H2AX foci facilitates the recruitment of MRN complex (MRE11, Rad50 and NBS) to the sites of DNA damage [56], further leading to the phosphorylation and activation of kinases, such as, ATM, Chk2, BRCA1 and Rad51 [57]. Interestingly, breast cancer cells harboring BRCA1 mutations are especially vulnerable to DNA damage causing agents due to their inherent inability to effectively repair DNA damage [58, 59] but their susceptibility to bacteria exposure has not been investigated. Hence, we examined the γH2AX foci formation and associated pathways in BRCA1 mutant breast cancer cells, HCC1937, SUM149 and MCF10A-BRCA1+/- cells. γH2AX foci were accompanied with the recruitment of RAD51 to the sites of DNA damage in cells exposed to *F. nucleatum* suggesting induction of repair pathways (Fig. 4c, d, Supplementary Fig. 6a). MCF10A-BRCA1+/- and HCC1937 cells were exposed to *F. nucleatum* for 4 hours followed by washing to remove extracellular bacteria and these cells were termed P0 cells. P0 cells were then cultured for several generations (P1, P2, P3) along with sham controls. Increased expression of XLF and Ku80 was observed in cells transiently exposed *F. nucleatum* as well as P0 and P2 cells (Fig. 4e). DNA-PKc is particularly involved in the repair of double-strand breaks (DSBs) through non-homologous end joining (NHEJ) which is considered error prone pathway. Intriguingly, DNA-PKc expression progressively increased from P0 to P2 MCF10A-BRCA1+/- and HCC1937 cells (Fig. 4e). We also observed a significantly higher nuclear expression of pATM along with loss of pBRCA1 in *F. nucleatum* co-cultured cells which remained consistent across two passages (Fig. 4f, g, Supplementary Fig. 6b, c). RNA-seq data showed enrichment of Defender Against Apoptosis (DAD1). Indeed, upon co-culturing HCC1937 and SUM149 cells with *F. nucleatum*, we observed an upregulation of DAD1 and CDK4 in the progeny cells (Fig. 4h, I, Supplementary Fig. 6d, e), suggesting an acquired survival advantage in these cells. These evidences suggest that *F. nucleatum* exposure leads to DNA damage and activation of NHEJ pathway, which may contribute to the growth and progression of breast cancer.

Breast cancer cells co-cultured with *F. nucleatum* exhibit prominent morphological and functional alterations. To understand the direct impact of the *F. nucleatum* on breast cancer cells, we co-cultured FN27236 and FN146CP with multiple breast cancer cell lines; luminal cell line MCF7, triple negative cell lines, HCC1806

and HCC1937 and inflammatory breast cancer cell lines SUM149 and MDA-MB-IBC3. *F. nucleatum* signal is detected in cells cocultured with *F. nucleatum* (Fig. 5a). All the cell lines exhibited an initial increase in cell death upon exposure to FN27236 and FN146CP with the percentage of cell death varying widely between 5% to 50% in different cells. Interestingly, after recovering from the initial shock response, MCF7 and HCC1806 second generation progeny cells (P2 cells) showed increased proliferation evident from cell viability assay (Fig. 5b, c) and clonogenicity (Fig. 5d). P2-HCC1937 and SUM149 cells also showed increased clonogenic potential (Fig. 5e). P2-MCF7 cells exhibited higher migration potential as demonstrated in a scratch-migration assay (Fig. 5f). Increased mammosphere formation was also noted for P2-MCF7 as well as P2-HCC1806 cells after being exposed to FN27236 and FN146CP (Fig. 5g, h). Demonstrating the impact of *F. nucleatum* exposure on migration and invasion potential, a higher number of P3-SUM149 cells migrated and invaded through transwell chambers and matrigel-invasion chambers, respectively (Fig. 5i). Together, these results show that a brief 4-hours exposure to *F. nucleatum* can impart higher growth, migration, invasion and stemness potential to breast cancer cells.

BRCA1-mutant breast epithelial cells exhibit elevated levels of Gal-GalNAc sugar residue. *F. nucleatum* is an anaerobic, non-motile, non-spore forming gram negative bacteria which targets tumor cells primarily through a lectin like interaction between its membrane adhesin, Fap-2 and tumor associated O-glycan Gal-GalNAc disaccharide residue which often gets unmasked and prominently expressed during transformation. Cells with higher Gal-GalNAc levels are more prone to *F. nucleatum* colonization [43, 60-62]. Mutations in several genes including TP53, PIK3CA, Kras and BRCA1/2 have been linked to increased risk of breast cancer [58, 59]. Among these, germline BRCA1 mutation ($BRCA1^{mut/+}$) is most prevalent with 1 in 400 women in USA carrying mutant BRCA1, and resultantly harboring a significant higher risk of breast cancer [59, 63]. We asked whether breast tumors harboring gene mutations are more susceptible to *F. nucleatum* colonization. Towards this, we used multiple derivatives of normal breast epithelial cell line, MCF10A (MCF10A-Kras, MCF10A-p53mut, MCF10A-p53/PIK3CA DKI, MCF10A-PI3Kmut and MCF10A-BRCA1+/-). Interestingly, PNA staining showed different levels of Gal-GalNAc sugar residue on each of these cells (Fig 5j). While Gal-GalNAc sugar residue was almost undetectable in MCF10A-parental cells, localization varied among the mutants. MCF10A- PIK3CAmut exhibited

nuclear accumulation of PNA while MCF10A-Kras showed cytoplasmic accumulation in few cells. Most strikingly, abundant cell surface accumulation of Gal-GalNAc sugar residue was observed in MCF10A-BRCA1+/- cells. Upon examining the breast cancer cell lines, MCF7 cells showed patchy accumulation in the nuclei while MDA-MB-231 cells presented uniform nuclear distribution but no surface accumulation. Lower level of cytoplasmic and cell surface distribution of PNA was observed in HCC1806 cells with very little presence in the nuclei. Most prominent surface accumulation of the sugar residue was observed in HCC1937 and SUM149 cells (Fig. 5j). Notably, of all breast cancer cell lines queried here, HCC1937 and SUM149 are the only ones harboring pathogenic BRCA1 mutation [64], suggesting an association between BRCA1 mutation and cellular O-glycosylation process. These results present an interesting possibility that breast tumors harboring BRCA1 mutation are more prone to *F. nucleatum* colonization and ensuing pro-cancer impact.

Cellular uptake and retention of *F. nucleatum* is proportional to the level of cell surface accumulation of Gal-GalNAc sugar residue in breast cells. To determine the extent of cellular uptake and intracellular retention of *F. nucleatum* in breast cancer cells, we used flow cytometry as well as high resolution confocal microscopy (Fig. 6). We tagged *F. nucleatum* with fixable membrane stain FM 143FX. The tagged bacteria were then co-cultured with cells with lower cell surface Gal-GalNAc levels (HCC1806 cells) as well as cells with high cell surface accumulation of Gal-GalNAc (HCC1937 and MCF10A-BRCA1+/- cells) for 4 hours. *F. nucleatum*-co-cultured cells were then washed, trypsinized, processed and analyzed by flow-cytometry (Fig. 6a). While all the cells tested were found to take up *F. nucleatum* initially as indicated by FITC positivity and increased SSC-A at 4 h post-removal of the bacteria, *F. nucleatum* was efficiently retained post 24h-removal of the bacteria in HCC1937 and MCF10A-BRCA1+/- cells (Fig 6a). To visualize cellular uptake of the bacteria, we co-cultured FM 1-43FX tagged FN27236 with MCF10A-BRCA1+/- cells for 4 hours followed by removal of the bacteria, washing, and incubating the cells for 16 hours. We then fixed the cells and imaged them at 40X, oil immersion. Rhodamine/Phalloidin was used to stain the cell cytoskeleton and DAPI was used as nuclear stain. Characteristic thin, rod-shaped, spindle-like morphology with pointed ends of *F. nucleatum* was clearly visible in MCF10A-

BRCA1+/- cells (Fig. 6b). To further confirm the internalization of *F. nucleatum* and retention within the cell, we used a combination of FM 143FX tagged FN27236 and anti-*F. nucleatum* antibody and performed dual immunofluorescence. MCF10A-BRCA1+/- cells were co-cultured with FM 1-43FX tagged FN27236 for 4 hours. The bacteria were removed from the cultures, washed, and fixed using 4% paraformaldehyde. Anti-*F. nucleatum* specific immunofluorescence was performed on non-permeabilized cells. Hoechst 33342 was used to counter stain the nuclei. FM 1-43FX tagged FN27236 internalized by the cells did not stain with anti-*F. nucleatum* antibody and continued to fluoresce green. FM 1-43FX tagged FN27236 which remained at the cell surface, on the other hand, were stained with anti-*F. nucleatum* antibody, hence, fluoresced both red and green (merged to yellow) (Fig. 6c). Finally, we questioned whether the bacteria would remain in the cells through multiple generations. To address this question, we co-cultured FN27236 with MCF10A-BRCA1+/- cells for 4 hours, trypsinized and sub-cultured the cells twice. The P2 (passage 2) cells were then fixed and permeabilized followed by immunofluorescence analysis using anti-*F. nucleatum* antibody. Intracellular *F. nucleatum* could be distinctly detected within the P2 cells confirming intracellular survival of *F. nucleatum* across generations (Fig. 6d). Taken together, our data suggests that breast cells with higher cell surface Gal-GalNAc residue exhibit increased cellular uptake and retention of *F. nucleatum*, and most importantly, a short 4-hour exposure to *F. nucleatum* results in sustained intracellular retention of bacteria across generations.

***F. nucleatum* accelerates growth, migration and stemness properties, and reduces treatment efficacy of MCF10A-BRCA1+/-cells.** Despite bearing one of the most common pathogenic BRCA1 mutations, 185delAG, resulting in a 2-bp deletion at the coding region close to the N terminus, MCF10A-BRCA1+/- cells are not tumorigenic. To truly explore the tumorigenic/ tumor promoting potential of opportunistic oral pathogen, *F. nucleatum*, we examined its influence on the functional properties of MCF10A-BRCA1+/- cells (Fig. 7). MCF10A-BRCA1+/- cells were exposed to *F. nucleatum* for 4 hours followed by washing to remove extracellular bacteria and these cells were termed P0 cells. P0 cells were then cultured for several generations (P1, P2, P3) along with sham controls. Cellular uptake of the bacteria led to increased clonogenicity in P0 cells, and the

clonogenic potential remained higher in P1 and P3 cells compared to respective sham-control cells (Fig. 7a). Anchorage-independent soft-agar colony formation assay was performed to query the potential tumorigenicity. P0-MCF10A-BRCA1+/- cells formed higher number of soft-agar colonies which were larger in size compared to sham-control cells (Fig. 7b). Exhibiting increased migration potential, P0-MCF10A-BRCA1+/- cells were significantly more motile than sham-control cells as evident from 3D spheroid migration assay (Fig. 7c) and expressed higher level of γ-H2AX puncta (Fig. 7d). Self-renewal or stemness is a key feature of cancer cells. We performed mammosphere formation assay as a measure of stemness. P0-MCF10A-BRCA1+/- cells were cultured in mammosphere forming media for a period of 7-10 days. The primary mammospheres formed by P0-MCF10A-BRCA1+/- cells were higher in number and larger in size as compared to the sham group. The primary mammospheres were then dissociated and re-seeded to form secondary and eventually tertiary mammospheres. P0-MCF10A-BRCA1+/- cells formed more and larger mammospheres in primary, secondary and tertiary assays suggesting an enrichment of stem-like cell population (Fig. 7e-f). Comparison to sham control cells, an increase in stemness in P0-MCF10A-BRCA1+/- cells was also confirmed by ALDH1 activity assay (Fig. 7g). To examine the tumor forming potential, we co-cultured MCF10A-BRCA1+/- cells with *F. nucleatum* for 24 hours (P0) and washed, trypsinized and sub-cultured (P1). We orthotopically implanted 5×10^6 P0 or P1 cells in mammary gland of NSG mice. Interestingly, very small, palpable tumor like nodules were formed by FN27236 infected MCF10A-BRCA1+/- cells after about 7 days while no such nodules were observed in the sham group. However, the tumor nodules did not progress to exponentially growing tumors and regressed on their own without any intervention in 14 to 20 days. IHC analysis of the tumors showed higher Ki67 and PCNA staining in the *F. nucleatum*- BRCA1+/- cells-derived tumor nodules (Supplementary Fig 7). Finally, we investigated the impact of FN27236 uptake on the drug sensitivity of cancer cells. We treated sham and P2-MCF10A-BRCA1+/- cells with Olaparib (0-100μM) and Doxorubicin (0-2μM) and performed cell viability (MTT) assay. FN27236 exposed P2-HCC1937, P2-SUM149 and P2-MCF10A-BRCA1+/- cells showed reduced sensitivity to both Doxorubicin and Olaparib (Fig. 7h). In HCC1937-Sham, in response to 100μM Olaparib, treated for 48 hours, 40.6% cells remained viable but viability was 61.2% in P2-FN-HCC1937 ($N=8$, $p<0.0001$). With same treatment, 31% of SUM149-Sham cells

remained viable while 41% were viable in P2-FN-SUM149 cells (N=8, $p<0.0001$). Similarly, in MCF10A-BRCA$^{+/-}$-Sham, ~20% cells remained viable but >40% cells remained viable in MCF10A-BRCA$^{+/-}$-FN cells after 48 hours treatment (N=8, $p= 0.0024$). When treated with Doxorubicin for 48 hours, at 1μM dose, viability of HCC1937-Sham was found to be 45.3% compared to 58.8% in P2-FN-HCC1937 cells (N=8, $p<0.0001$); viability of MCF10A-BRCA$^{+/-}$ cells increased from 49.3% to 57.1% in MCF10A-BRCA$^{+/-}$-FN cells (N=8, $p<0.0001$). However, FN did not impact the response of SUM149 to Doxorubicin (Fig 7h). These results suggest that intra-tumoral *F. nucleatum* might reduce response to therapy in breast cancer patients.

Discussion

A growing body of evidence supports a complex interplay between the microbiota and breast cancer development and progression, and distinct microbial perturbations in gut and breast microbiota associated with benign and malignant breast cancer have been noted [4, 6-9, 65, 66]. In addition to breast and gut microbial dysbiosis, alterations in oral microbiota are now recognized as potential contributors to various systemic diseases, including several types of cancer. One particularly notable oral bacterium gaining significant attention in cancer research is *F. nucleatum*. [26-41].This anaerobic, gram-negative microbe is commonly found in human dental biofilm. Its involvement in periodontal disease, a prevalent inflammatory condition affecting the supporting structures of the teeth, has been well-established [15-18]. However, emerging evidence suggests that *F. nucleatum*'s influence extends beyond the oral cavity, potentially playing a role in distant cancers, including breast cancer. In this study, we aimed to address the question if this bacterium possesses a tumor initiating potential and if it can be considered as a breast cancer risk factor. We found the presence of *F. nucleatum* in benign and malignant breast cancer samples using meta-analysis of clinical data, and then developed *in vivo* approaches to examine its involvement in breast tumorigenesis. Since oral microbiota has been proposed to impact distant target organs using hematogenous transmissions [42], we investigated whether *F. nucleatum* impacts breast cancer when administered systemically via tail-vein injections. Indeed, hematogenous administration of *F. nucleatum* significantly increased breast tumor growth and lung metastasis. Tumor dissociated cells exhibited the attainment of a highly migratory, invasive, stemness-rich phenotype that is supported by the drastic change in the molecular machinery as expression of the genes supporting metastatic growth is induced in *F. nucleatum*-exposed cells. Several cancer types including head and neck, pancreatic and oral cancer show increased incidence, aggressiveness and therapy resistance in response to *F. nucleatum* [26-41]. Breast cancer models, upon *F. nucleatum* administration, have also shown increased growth of existing tumors as well as modulation of tumor microenvironment [42-44]. Although these studies establish the effect of *F. nucleatum* on growth and metastatic progression of existing tumors, its biological impact on breast cancer initiation in healthy breast is unknown. Using a mouse intraductal (MIND) model to imitate the colonization of healthy mammary ducts with *F.*

nucleatum, we, for the first time, have demonstrated that exposure to *F. nucleatum* causes the formation of metaplastic and hyperplastic lesions in healthy NSG and BALB/c mice within three weeks. These lesions presented with high severity score calculated based on the extent of inflammation, presence of some giant multinucleated cells, granulated mast cells, macrophages and neutrophils, as well as lipofuscin and collagen accumulation. Our results show that direct mammary ductal-colonization with *F. nucleatum* is sufficient to initiate metaplastic lesions within three weeks of microbe exposure in healthy mice, and hematogenous route potentiates existing mammary tumor growth and metastatic progression along with activation of an oncogenic signaling cascade.

F. nucleatum expresses a large outer-membrane autotransporter/lectin protein Fap2, which functions as Gal-GalNAc binding lectin. In transformed cells, dysregulation of O-glycosyltransferases such as GALNT family members initiates aberrant and truncated mucin-type O-glycosylation leading to surface accumulation of disaccharide, D-galactose–β(1-3)-N-acetyl-D-galactosamine (Gal-GalNAc). Host cell Gal-GalNAc acts as homing signal for *F. nucleatum* and level of the disaccharide expression has been shown to be proportional to cellular uptake of the bacteria, and the bacterial FadA protein then interacts with E-cadherin present on the mammalian cells [43, 60-62] inducing downstream oncogenic pathways. We, therefore, envisioned that breast cells with higher Gal-GalNAc levels may be more amenable to *F. nucleatum* colonization. Breast cancer is a heterogenous disease associated with mutations in several genes such as TP53, PIK3CA, Kras and BRCA1/2 [58, 59]. Among these, BRCA1 mutations are most frequently detected in familial breast cancers. However, 30-45% of women with inherited BRCA1 mutations do not develop breast cancer indicating that additional factors might also play a role in cancer initiation in genetically susceptible individuals. Among breast epithelial cells harboring a variety of mutations, most abundant cell surface accumulation of Gal-GalNAc sugar residue was observed in MCF10A-BRCA1+/- cells. Also, breast cancer cells harboring pathogenic BRCA1 mutations exhibited highest cell surface accumulation of Gal-GalNAc sugar residue compared to other breast cancer cells. These results indicate that breast epithelial cells harboring BRCA1 mutation can be more vulnerable to *F. nucleatum* colonization which may serve as the additional environmental hit and induce tumor initiation and progression. Intriguingly, we successfully showed the internalization and retention of *F. nucleatum* in BRCA1 mutant breast

epithelial and breast cancer cells. These are the first observations connecting *F. nucleatum* exposure with cellular uptake and retention in BRCA1 mutant cells. Intratumoral bacteria have been shown to reside within the cells in the perinuclear regions and promote metastatic dissemination of breast cancer cells [67].Owing to the connection between periodontal disease and *F. nucleatum*, our intriguing results pose a larger question- whether periodontal disease increases the risk of breast cancer in women harboring BRCA1 mutations. Microbial dysbiosis is now appreciated as an important risk factor that shares a direct/indirect connection with many established risk factors for breast cancer such as age, obesity, cumulative estrogen exposure, alcohol exposure, and breast density [68, 69], our results, for the first time, connect an oral pathogenic bacteria with a genetic risk factor.

The microbiota has been shown to aid in breast tumorigenesis via a multitude of mechanism like exposure to endotoxins and microbial metabolites, activation of TLR and NLR dependent pathways, immune modulation, TME modification, disruption of intercellular communication, cytokine activation and induction of DNA damage [70]. *F. nucleatum* has been shown to promote migration and metastasis in colorectal cancer via miR-1322/CCL20 axis and M2 polarization [71], ALPK1/NFκB/ICAM1 axis [72], downregulation of m^6A methyltransferase METTL3 [73], induction of IL8 and CXCL1 secretion [74] and upregulation of MMP7 via activation of MAPK(JNK)-AP1 axis [75]. Our results advance the understanding of the molecular mechanisms underlying *F. nucleatum* and breast cancer progression. RNA-seq analyses of tumors developed in mice administered with *F. nucleatum* show perturbations of genes associated with DNA damage and repair pathway. Double-stranded break (DSB) in the genome of mammalian cells activates the DSB sensors and modulates DNA damage pathway. We observed increased γ-H2AX foci in *F. nucleatum* exposed cells which can facilitate the recruitment of MRN complex (MRE11, Rad50 and NBS) to the sites of DNA damage [56] and trigger phosphorylation and activation of kinases, such as, ATM, Chk2, BRCA1 and Rad51 [57]. Also, BRCA mutant cells, MCF10A-BRCA1+/- and HCC1937, exhibited elevated expression of DNA-PKc upon *F. nucleatum* exposure which was further increased in progeny cells. This observation has important implications on the NHEJ mechanism as DNA-PKcs are DNA dependent protein kinases which are the key enzymes of DNA repair, particularly through the error prone NHEJ mechanism. DNA-PKcs are a group of pro-tumorigenic protein kinases known to phosphorylate more than 700

proteins and their upregulation is associated with cancer progression and resistance to chemotherapy and radiation [76]. In addition to its role in DNA repair, DNA-PKcs have been shown to have a multitude of non-canonical functions including transcriptional regulation, telomere maintenance, metabolic regulation, and immune signaling making it an important and emerging therapeutic target. Taken together our results suggests that cellular uptake of *F. nucleatum* induces DNA damage in the host cells triggering a cascade of error prone DNA repair events primarily via NHEJ mechanism. There is an accumulation of endogenous DNA-damage events across generations leading to upregulation of DNA-PKcs which in turn activate downstream defense mechanism making the cells more aggressive and resistant to chemotherapeutics.

Collectively, these results present new insight into the relationship between an oral pathogenic microbe *F. nucleatum*, breast carcinogenesis, and DNA damage and repair pathway. Our study is the first to show that BRCA1 mutant breast cancer cells may be more vulnerable to *F. nucleatum* owing to their increased ability for internalization and retention of the bacteria. This is an exciting observation which needs additional studies to clarify the clinical connection between periodontal disease, increased colonization of *F. nucleatum* in oral cavity and breast tissue, and development of breast cancer in women harboring BRCA1 mutations. It is indeed a challenging yet motivating goal that may help unravel novel contributors to the pathogenesis of breast cancer and develop a better understanding regarding the interconnectivity of multiple established and novel risk factors.

Methods

Cell lines and bacterial strains Breast cancer cell lines MCF7, HCC1806, HCC1937, SUM149, and normal breast epithelial cell line MCF10A were procured from the ATCC. MCF10A-Kras, MCF10A-p53mut, MCF10A-PIK3CAmut, MCF10A-BRCA1+/- and MCF10A-DKI cells were a gift from Dr. Ben Park (Vanderbilt-Ingram Cancer Center). MDA-MB-IBC3 cells were a gift from Dr. Wendy Woodward (MD Anderson Cancer Center). Cells were maintained at 37°C and 5% CO_2, and were used for experiments within 10 to 20 passages. All cells were authenticated via short tandem repeat testing. *Mycoplasma* detection was routinely performed using the MycoAlert Detection Kit (LT07-218, Lonza, Bend, OR, USA). Cultures of *Fusobacterium nucleatum* strain FN27236 (ATCC strain) and FN146CP (CRC patient derived strain) were maintained anaerobically at 37°C in BHI medium [37 g of brain heart infusion base (Difco Laboratories)/liter, 5 g of yeast extract (Difco Laboratories, Detroit, MI)/liter, and 1 μg of vitamin K/mL, 5 μg of hemin/mL, and 0.5 g of l-cysteine/mL] from Anaerobe Systems (Morgan Hill, CA). Bacterial pellets were washed and resuspended with 1 × Dulbecco PBS (1 × PBS free of calcium chloride and magnesium chloride) for mouse inoculums.

Antibodies and reagents Anti-*F. nucleatum* antibody was a generous gift from Dr Daniel J. Slade (Virginia Tech). For Western blot and IHC, rabbit monoclonal anti-γH2AX, anti–Ki67, anti-CD45, anti-CD4, anti-PCNA, anti-Oct4, anti-Nanog, anti-CDK4, anti-tubulin antibodies were purchased from Cell Signaling Technology (Danvers, MA). Anti-β-catenin antibody and anti-CD3 antibodies were purchased from Santa Cruz Biotechnology (Dallas, TX) and DAKO Agilent (Santa Clara, CA), respectively. Anti-RAD51, anti-Transferrin and anti-DAD1 antibodies were purchased from Thermo Fisher Scientific (Waltham, MA). Vectastain IHC kit was purchased from Vector laboratories Inc (Newark, CA) and mouse monoclonal β-actin was procured from Sigma-Aldrich (St. Louis, MO). Horseradish peroxidase–conjugated goat anti-rabbit IgG, goat anti-mouse IgG and donkey anti-goat IgG were purchased from Sigma-Aldrich (St. Louis, MO). Chemiluminescent peroxidase substrate and 3-(4,5-dimethylthiazol-2-yl)-2,5-diphenyltetrazolium bromide (MTT), FITC conjugated lectin from *Arachis hypogaea* (PNA) and FM™ 1-43FN fixable analog of FM™ 1-43 membrane stain were procured from Sigma-Aldrich (St. Louis, MO). Rhodamine Phalloidin was procured from Invitrogen Corporation (Waltham, MA).

***In Silico* analysis** Raw data from PRJNA335375 study examining buccal, skin swab, skin tissue and breast tissue microbiota of women with malignant breast cancer and benign breast disease, and RNA sequencing data set GSE144143 were accessed from NCBI SRA. 16SrRNA sequence analysis was performed using QIIME module and bulk-RNA sequence analysis was performed using DESeq2 followed by GSEA analysis.

RNA-Sequencing and Data Analysis Total RNA was extracted from tumors from *F. nucleatum* and sham-control group. Library preparation was performed using the TruSeq Stranded Total RNA with Ribo-Zero Human/Mouse/Rat kit (Illumina, San Diego, CA). Libraries were sequenced on the NovaSeq X Plus platform (10B or 25B flow cell, 150 bp paired-end reads) (Illumina, San Diego, CA). Raw BCL files generated from the sequencer were converted to FASTQ format using bcl2fastq v2.20.0 (Illumina). Reads were quality trimmed and adapter sequences were removed using TrimGalore v0.6.3. Aligned reads and gene/transcript-level quantification were performed using RSEM v1.3.0 with the hg38 reference genome. Differential gene expression analysis between co-cultured and control samples was conducted with DESeq2 [77] via the iDEP2.0 portal [78]. KEGG pathway enrichment was analyzed through iDEP2.0. Normalized read counts were further analyzed by Gene Set Enrichment Analysis (GSEA) [79] to perform enrichment of DNA-damage and repair pathways, and a metastasis gene signature (see Supplementary Table 1 for gene sets). Heatmaps were created through customized python script and Broad institute Morpheus (https://software.broadinstitute.org/morpheus). Pathway enrichment results were plotted through a customized R script and SR-plot (https://www.bioinformatics.com.cn/en).

Mammary gland inoculation of *F. nucleatum* All animal studies were in accordance with the guidelines of Johns Hopkins University Animal Care and Use Committee. For mammary gland colonization, twice parous BALB/c mice were obtained from Charles River Laboratories (Rockville, MD) and maintained in-house. Mice were given antibiotic cocktail (clindamycin 0.1 g/L and streptomycin 5 g/L) in water bottles (Hospira and Amresco) for 7 days and discontinued. Mice were also injected with antibiotic cocktail intraductally to clear ductal microbiome at the same time. *Fusobacterium nucleatum* strain FN27236 and FN146CP cultures were sub-cultured and incubated at ~OD_{600nm} 0.05; between 24-36h, the culture obtains an ~OD_{600nm} of 1.0-1.2. Bacterial pellets were washed with oxygen reduced PBS Mice in FN27236 and FN146CP group were then injected with

0.5×10^8 CFUs of bacteria in 20µl sterile, oxygen reduced PBS via intraductal administration. For sham control, mice were intraductally injected with 1× PBS (20µl). Animals were monitored daily for signs of infection or mastitis.

Breast cancer xenograft model and intravenous bacterial inoculation NSG mice (female, 6–8 weeks old) were acquired from Sidney Kimmel Comprehensive Cancer Center (SKCCC) animal facility and maintained in-house. Exponentially growing, 4×10^6 HCC1806 breast cancer cells were implanted in the mammary glands of NSG mice. Once palpable tumors were observed, we inoculated 1×10^8 CFUs of FN27236 or FN146CP by tail vein injection. Sterile saline was used as vehicle control. Tumor volumes were monitored. Tumors were excised and processed for further analysis.

Mammalian cell-*F. nucleatum* co-culture *Fusobacterium nucleatum* strain FN27236 and FN146CP were cultured for 24-hour followed by sub-culturing in oxygen-reduced BHI media from Anaerobe Systems (Morgan Hill, CA) and allowed to grow to OD 1-1.2 in anaerobic hood. Bacterial culture (300µl) was centrifuged and bacterial pellets were washed with oxygen reduced PBS and resuspended in 1ml PBS. MCF7, HCC1806, HCC1937, SUM149, MDA-MB-IBC3, MCF10A, MCF10A-Kras, MCF10A-p53mut, MCF10A-PIK3CAmut, MCF10A-BRCA+/- and MCF10A-DKT cells were cultured in respective media overnight. The cells were washed twice with PBS followed by incubation in antibiotic free, serum free media. An aliquot of bacterial supernatant was added to the cells (50µl bacterial supernatant/ 1ml of culture media) followed by incubation at 37°C for 4 hours. After 4 hours, the media was replaced with regular culture media and cells were incubated for 16 hours. These cells were designated as P0 cells for further experiments. The P0 cells were trypsinized and reseeded to obtain P1, P2 and P3 cells subsequently (P= Passage number).

Cellular uptake of bacteria and visualization of intracellular bacteria *For Flow cytometry*, *F. nucleatum* were tagged by inoculating with fixable membrane stain FM 143FX for 5 minutes. The bacteria were then washed twice with oxygen reduced PBS. The tagged bacteria were co-cultured with MCF10A-BRCA+/- breast cancer cells. Co-cultured cells were washed, trypsinized, processed and analyzed by flow-cytometry for FITC positivity.

To visualize cellular uptake of the bacteria using immunocytochemistry, FM 1-43FX tagged FN27236 was co-cultured with MCF10A-BRCA+/- cells for 4 hours followed by removal of the bacteria containing media, washing with PBS and incubation for 16 hours. Cells were fixed and imaged at 40X, oil immersion. Rhodamine/Phalloidin was used to stain the cellular cytoskeleton and DAPI was used as nuclear stain. *To confirm the internalization of bacteria and retention within the cell*, anti-*F. nucleatum* antibody was used. FM 1-43FX tagged FN27236 was co-cultured with MCF10A-BRCA+/- cells for 4 hours followed by removal of the bacteria containing media, washing with PBS and incubation for 16 hours. Bacteria-exposed cells were trypsinized and sub-cultured twice to achieve P2 cells. The P2 cells were then fixed, permeabilized and immunofluorescence was performed using anti-*F. nucleatum* antibody. Dual immunofluorescence was performed using FM 143FX and anti-*F. nucleatum* antibody. *To further confirm the internalization of bacteria*, MCF10A-BRCA+/- cells were co-cultured with FM 1-43FX tagged FN27236 for 4 hours. The bacteria were removed from the cultures, and cells were washed and fixed using 4% paraformaldehyde. Anti-*F. nucleatum* specific immunofluorescence is performed on non-permeabilized cells. Hoechst 33342 was used to counter stain the nuclei.

Immunohistochemistry Tumor tissue sections were fixed in 10% formalin, paraffin-embedded and sectioned. IHC analyses of the tissue sections was carried out with anti-Ki67, anti-Pan-keratin, anti-CD45, anti-CD3, anti-CD4 and anti-phospho-γ-H2A.X antibodies, followed by incubation with HRP-conjugated secondary antibodies and developed using DAB peroxidase substrate kit (SK-4100, Vector Laboratories Inc, Newark, CA). Images were captured with a Leica microscope at 20× magnification. Images were analyzed by Aperio ImageScope Software, Leica Biosystems (Deer Park, IL). Quantification of micrographs and IHC was done using Aperio ImageScope, Leica Biosystems (Deer Park, IL).

Immunofluorescence For immunofluorescence, fixed cells were permeabilized using 0.1% Triton-X-100 followed by overnight incubation with primary antibody at 1:100 dilution in 3% BSA. Cells were then incubated with FITC/TRITC-tagged secondary antibody. Cells were examined under Leica E800 fluorescent microscope. Images were captured at 40× magnification using oil immersion objective with Leica Elements software (Leica Biosystems, Deer Park, IL).

Mammosphere assay For liquid mammosphere assay, 5,000 FN-cocultured cells were seeded in 2 mL of liquid mammosphere media in 30 mm ultra-low attachment plates and allowed to grow for 7 days. The mammospheres were resuspended to make single cell suspensions and reseeded to form 2°and 3°mammospheres. Cultures were observed under microscope and spheres (>50 μm) were counted.

Spheroid-migration assay To make 3D spheroids, 96-well plate was coated with 0.5% agar and allowed to solidify. 2×10^4 cells in 200μl of media per well were seeded. The plate was incubated on gently rotating platform in the incubator at 37°C and 5% CO_2 for 48 hours allowing the cells to grow in solid spheres. The spheres were then picked and planted on 2D plates in antibiotic free culture media with or without *F. nucleatum*. Spheres were allowed to adhere for 5-6 hours and then the media was replaced with normal growth media. Spheres were imaged and migration of single cells from the tumor spheroids over time was monitored using phase-contrast microscopy. Distance migrated was measured using Aperio ImageScope Software, Leica Biosystems (Deer Park, IL) and plotted as a measure of cell movement using GraphPad Prism 5 software.

Matrigel-invasion, transwell-migration, and scratch-migration assays To assess the migratory and invasive potential of *F. nucleatum* co-cultured cells, we utilized the Matrigel-invasion, scratch-migration, and transwell-migration assays. P0, P1 and P2 cells were used to perform the assays. *For Matrigel-invasion assay*, 50,000 cells were seeded in a Matrigel invasion chamber from BD Biocoat Cellware (Corning, Corning, NY). *For transwell-migration assay*, 20,000 cells were seeded in the top chamber with an 8-μm pore size, and cells were allowed to invade or migrate through the Matrigel or filter for 24 to 48 hours. On the top chamber, the cells were seeded in serum free media while the bottom chamber had 10% FBS supplemented media. The number of invaded/migrated cells on representative sections of each membrane was counted under light microscope. *For scratch-migration assay*, monolayers of P0, P1 and P2 cells were allowed to form; a 1-mm wide scratch was made across the cell layer using a sterile pipette tip, and media were replaced with fresh media. Plates were photographed immediately after scratching, and migration of cells was followed for various time intervals. Wound closure was quantified from distance between edges using Aperio ImageScope Software, Leica Biosystems (Deer Park, IL). Speed of migration was calculated, and wound closure was plotted using GraphPad Prism 5 software [80, 81].

Detection of cancer stem cell markers by flow cytometry Stemness was estimated by measuring aldehyde dehydrogenase (ALDH) activity of Sham and *F. nucleatum* treated cells by flow cytometry. ALDEFLUOR^{TM} Kit from STEMCELL technologies (Seattle, WA) was used. Assays were conducted as per manufacturer's instructions.

Protein isolation and western blotting Whole-cell lysates were prepared using modified RIPA buffer. For protein lysates of tumor samples, tumor tissues were homogenized using a tissue homogenizer in mammalian tissue lysis buffer on ice.

RT-PCR For RT-PCR, cells were lysed in TRIzol, RNA was isolated by chloroform-isopropanol method, and cDNA was synthesized using an iScript cDNA Synthesis Kit. qPCR was performed.

Statistical Analysis All experiments were performed in triplicates. Measurements of micrographs and IHC quantitation were done using Aperio ImageScope, Leica Biosystems Statistical analyses were done using GraphPad Prism 5. ICC images were quantified using Image J software. Results were considered to be statistically significant if $P < 0.05$. Results were expressed as mean ± SE between triplicate experiments performed thrice. For comparison between multiple groups, statistical significance was determined by one-way ANOVA and Bonferroni analysis. Comparison between two groups was done using the Student's *t* test. Two-way ANOVA was used to compare drug response curves.

Legends to Figures

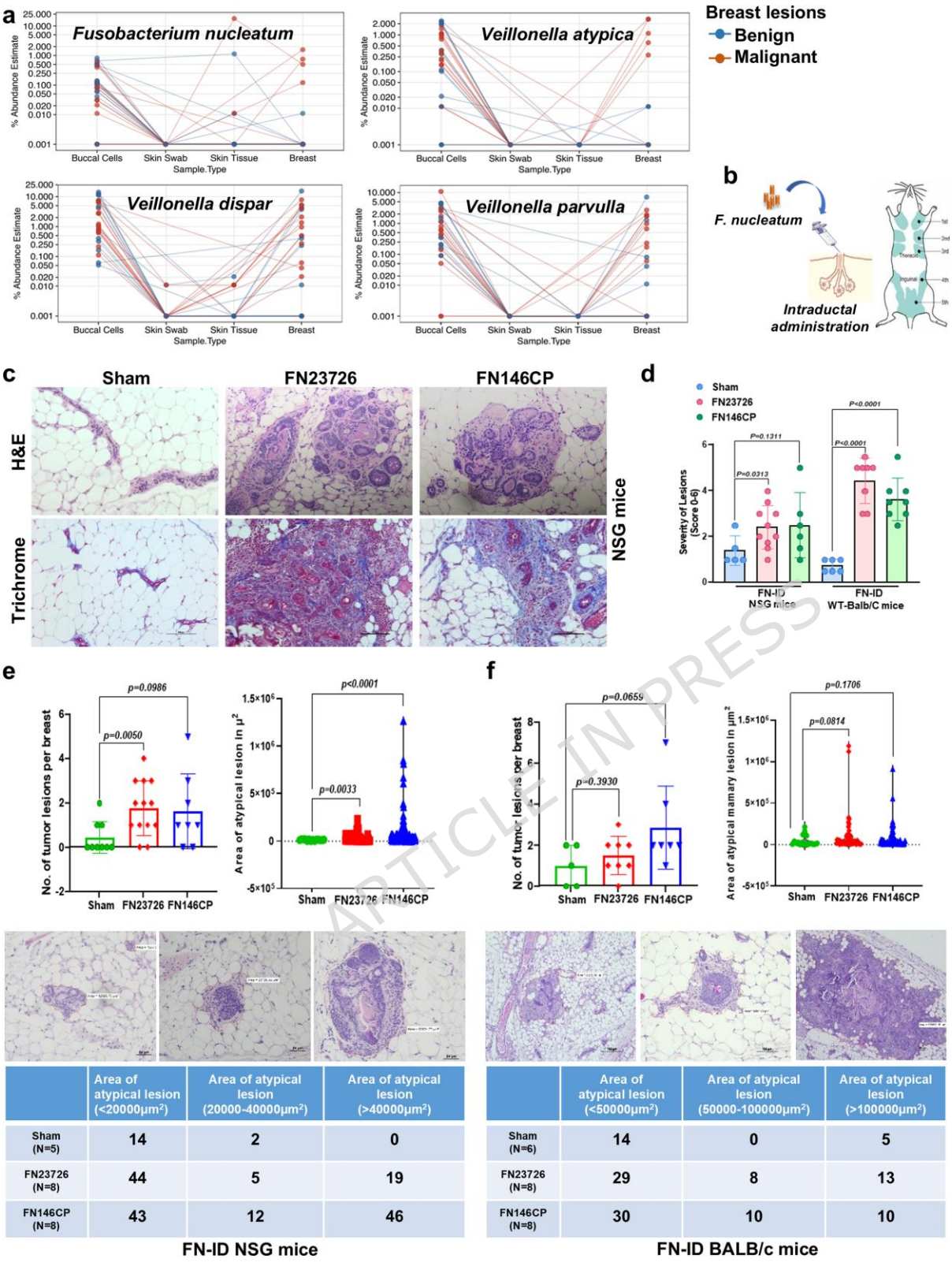

	Area of atypical lesion (<20000µm²)	Area of atypical lesion (20000-40000µm²)	Area of atypical lesion (>40000µm²)
Sham (N=5)	14	2	0
FN23726 (N=8)	44	5	19
FN146CP (N=8)	43	12	46

FN-ID NSG mice

	Area of atypical lesion (<50000µm²)	Area of atypical lesion (50000-100000µm²)	Area of atypical lesion (>100000µm²)
Sham (N=6)	14	0	5
FN23726 (N=8)	29	8	13
FN146CP (N=8)	30	10	10

FN-ID BALB/c mice

Figure 1. Intraductal colonization with *F. nucleatum* leads to the formation of metaplastic lesions in mammary glands of healthy mice. (a)16S-rRNA sequence analysis of buccal cavity, skin swab, skin tissue and breast tissue of women with benign and malignant breast cancer shows many oral microbes overlapping with

breast tumors. **(b)** Schematic representation of intraductal administration of *F. nucleatum* in mice. **(c)** Representative images of H&E and Trichrome-stained mammary gland tissue from NSG mice harboring intraductal colonization with *F. nucleatum*. **(d)** Dot plot shows the scoring for the severity of lesions (on a scale of 0-5) in NSG and wild type-Balb/C mice bearing intraductal colonization of *F. nucleatum* ATCC strain 27236 or the strain derived from human colorectal cancer FN146CP. **(e, f)** Dot plot showing the number of tumor lesions per mammary gland and the violin plot showing the area of atypical lesions detected in mammary glands of NSG mice **(e)** and Balb/C mice **(f)** intraductally colonized with *F. nucleatum* ATCC strain 27236 or the strain derived from human colorectal cancer FN146CP. *Lower panels:* Representative H&E-stained sections and corresponding scoring of atypical lesions detected in mammary glands of NSG mice **(e)** and Balb/C mice **(f)** intraductally colonized with *F. nucleatum* strain 27236 or strain FN146CP.

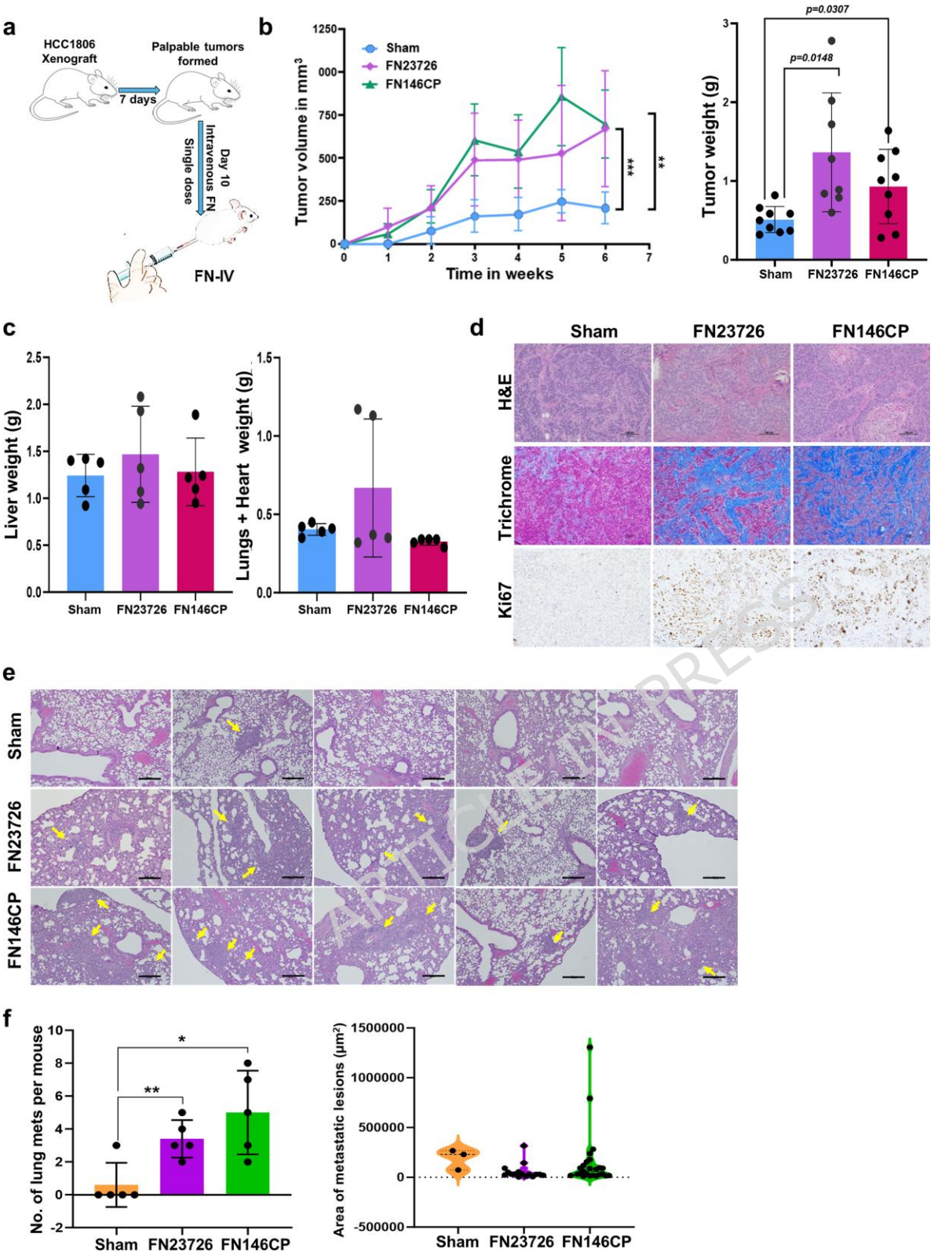

Figure 2. *F. nucleatum* increases breast cancer growth and lung metastasis when administered via hematogenous route. (a) Schematic for the experiment. HCC1806 xenograft was established by implanting

4×10^6 HCC1806 cells in the mammary fat pads of mice. Palpable tumors appeared at day 7. Once all mice had palpable tumors, a single inoculum of 1×10^8 CFUs of FN146CP or FN27236 was administered intravenously via tail vein. **(b)** Line graph and bar graph show tumor volume and tumor weight of HCC1806-derived tumors in mice intravenously administered with *F. nucleatum* FN27236 or FN146CP. **(c)** Liver, lungs and heart were not impacted upon intravenous administration of *F. nucleatum* FN27236 or FN146CP in mice. **(d)** Representative images of H&E staining and Trichrome-stained and Ki67-stained HCC1806-derived tumor sections from mice intravenously injected with *F. nucleatum* FN27236 or FN146CP. **(e, f)** Representative images and quantification of H&E staining of lungs from HCC1806-derived tumor bearing mice intravenously administered with *F. nucleatum* FN27236 or FN146CP. Every H&E image is representative of one mouse (N per group=1).

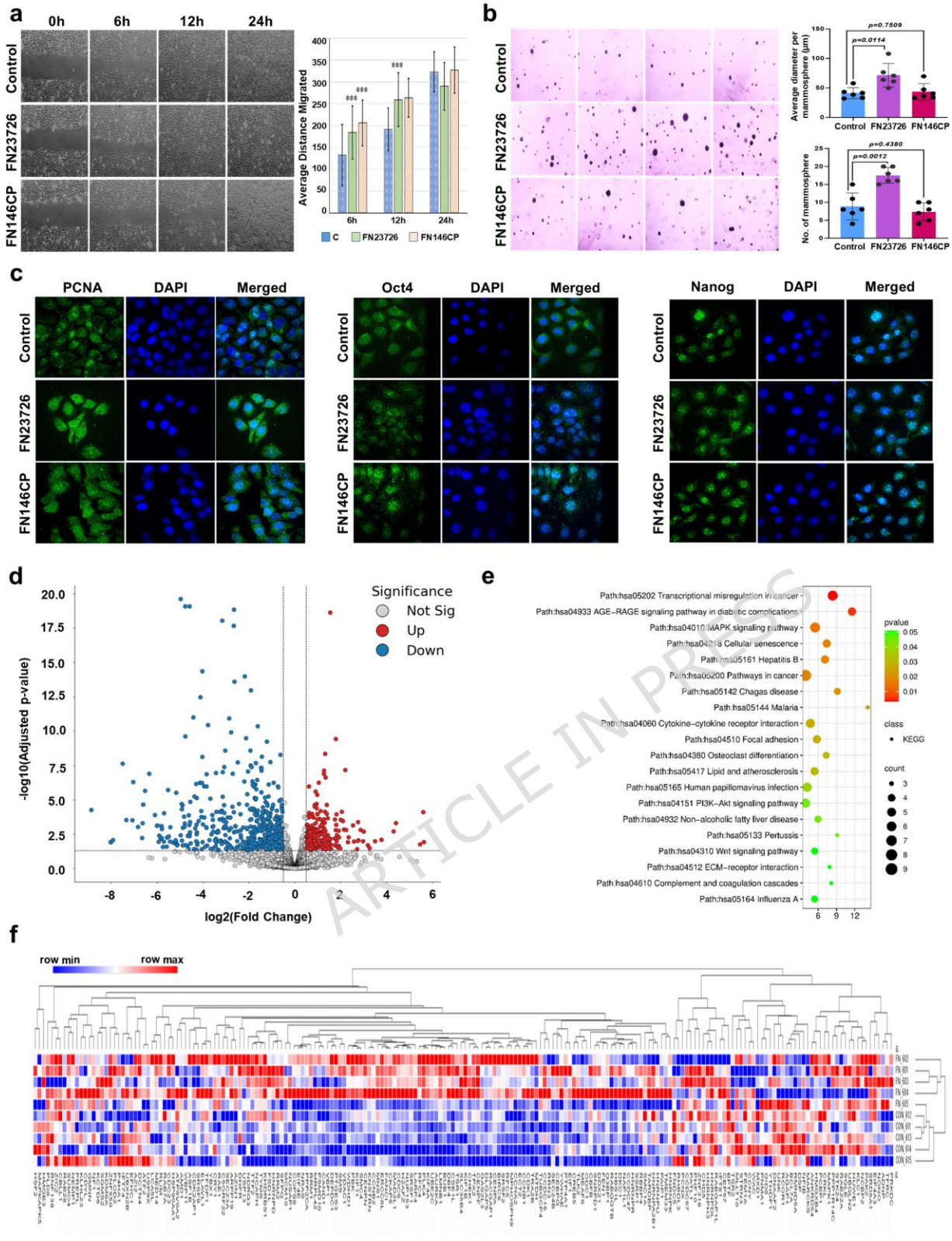

Figure 3. Tumor-dissociated cells from *F. nucleatum* exposed tumors exhibit increased mammosphere, and *F. nucleatum* exposure modifies several important pathways. (a) Representative images of tumor-dissociated cells, from HCC1806-derived tumors developed in mice intravenously injected with *F. nucleatum* FN27236 or

FN146CP, migrating in a wound-healing assay. Bar graph shows average distance migrated. **(b)** Representative images of mammospheres formed with the tumor-dissociated cells from HCC1806-derived tumors developed in mice intravenously injected with *F. nucleatum* FN27236 or FN146CP. Bar graphs show the average diameter and number of mammospheres formed with the tumor-dissociated cells from HCC1806-derived tumors developed in mice intravenously injected with *F. nucleatum* FN27236 or FN146CP. **(c)** Representative images of immunocytochemical analyses of PCNA, Oct4 and Nanog expression in the tumor-dissociated cells from HCC1806-derived tumors developed in mice intravenously injected with *F. nucleatum* FN27236 or FN146CP. **(d)** Volcano plot showing differential gene expression patterns in control and FN treated tumors. **(e)** KEGG pathways differentially regulated in FN treated tumors. **(f)** Heat map showing upregulation of breast cancer metastasis pathway genes in FN infected breast tumor models.

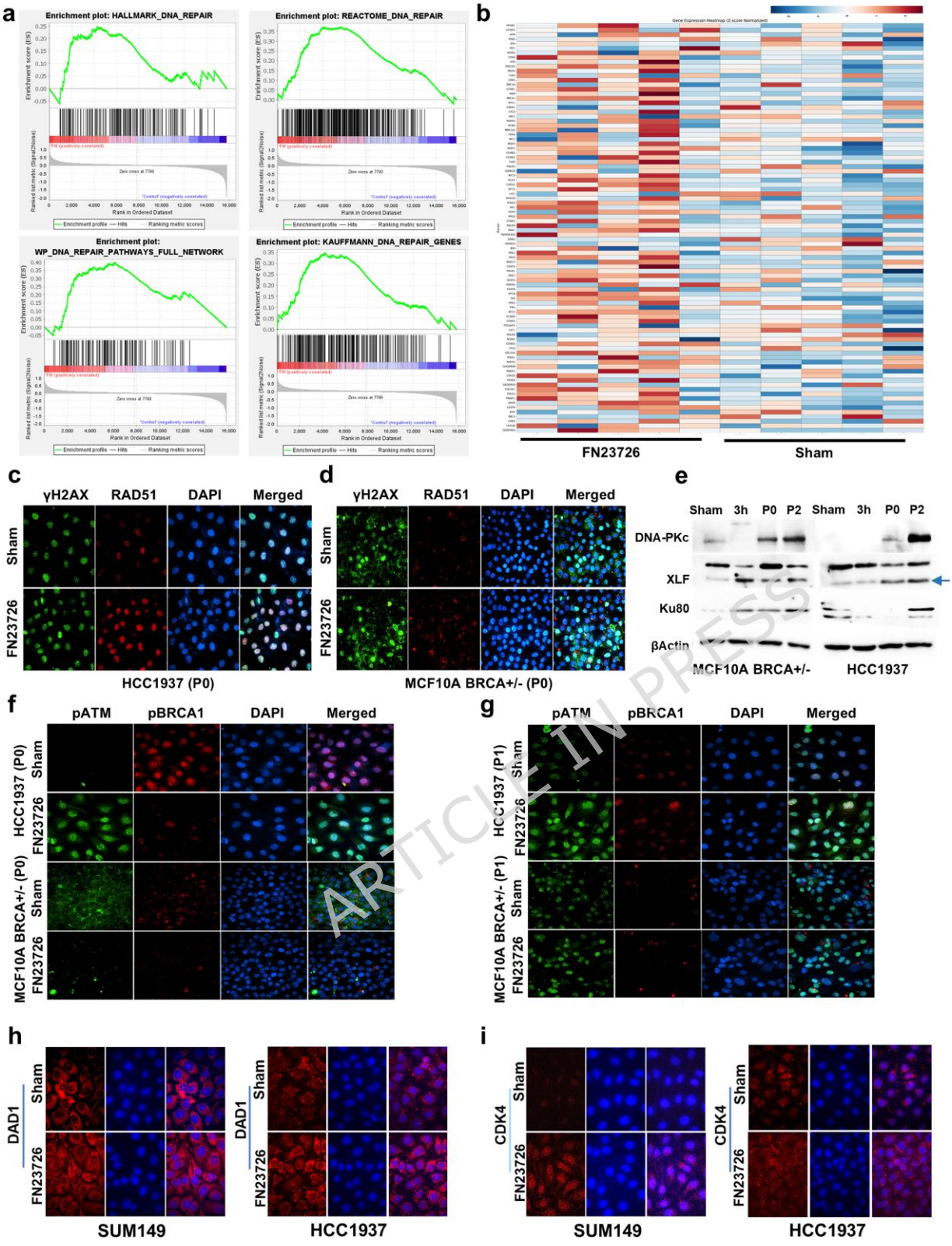

Figure 4. ***F. nucleatum*** **induces DNA damage leading to upregulation of error prone NHEJ repair pathway.**

(a) GSEA analysis from bulk-RNA sequencing of HCC1806 xenografts with intravenous FN27236 inoculation showing activation of DNA repair pathways. (**b**) Heatmap showing relative expression of genes involved in DNA

damage and repair in FN infected breast tumors. **(c, d)** Representative immunocytochemistry images showing HCC1937 (**c**) and MCF10A-BRCA+/- **(d)** P0 cells exposed to *F. nucleatum* FN27236 and stained with γH2AX and RAD51 antibodies, as indicated. DAPI is used to stain the nuclei. **(e)** Immunoblots showing the expression of DNA-PKc, XLF and Ku80 in MCF10A-BRCA+/- and HCC1937 cells exposed to *F. nucleatum* FN27236 for 3 h and P0 (passage 0) or P2 (passage 2) cells. **(f, g)** Representative immunocytochemistry images showing HCC1937 and MCF10A-BRCA+/- P0 **(f)** and P1 **(g)** cells exposed to *F. nucleatum* FN27236 and stained with pATM and pBRCA1 antibodies, as indicated. DAPI is used to stain the nuclei. **(h-i)** Representative immunocytochemistry images showing SUM149 **(h)** and HCC1937 **(i)** cells exposed to *F. nucleatum* FN27236 and stained with DAD1 and CDK4 antibodies, as indicated. DAPI is used to stain the nuclei.

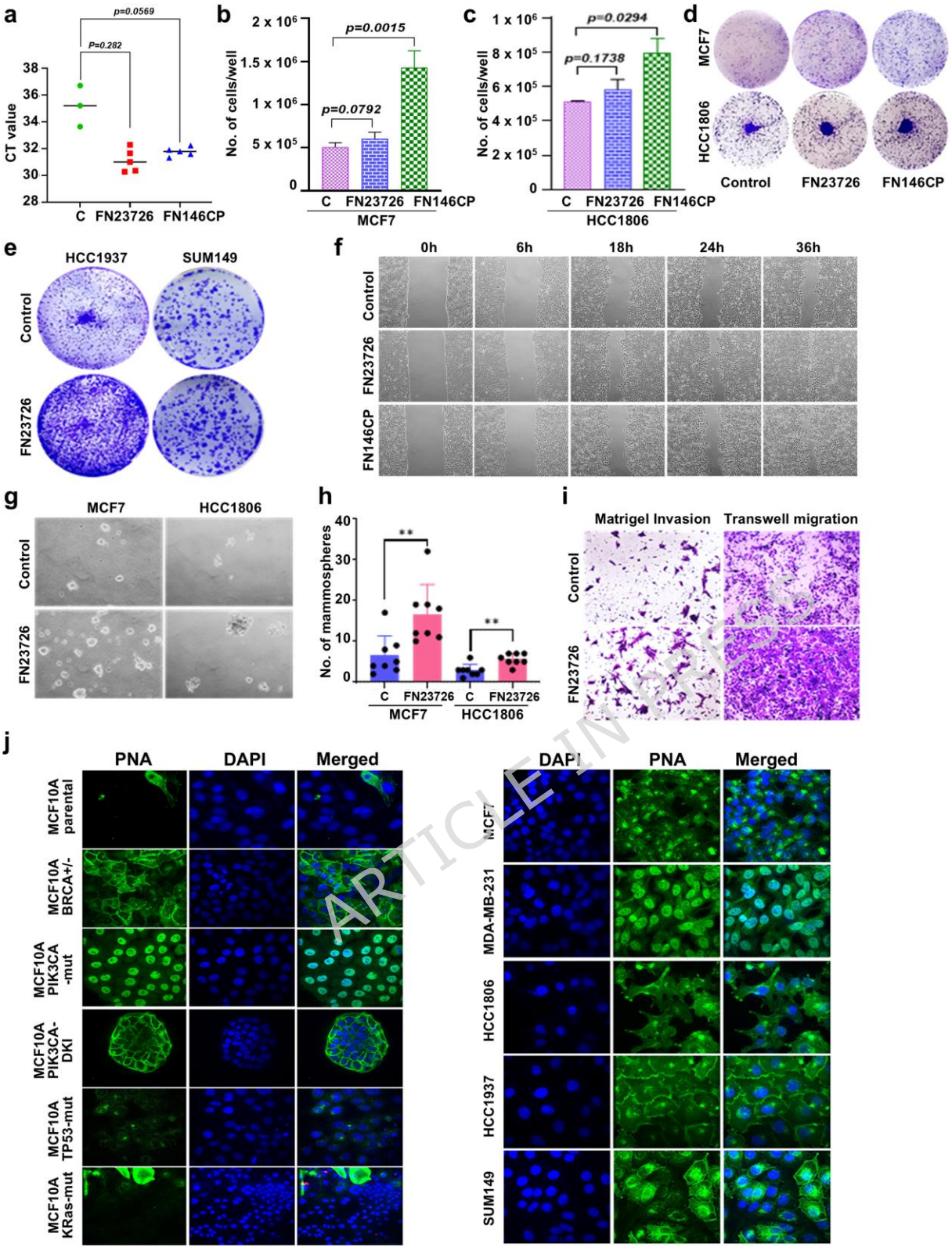

Figure 5. *F. nucleatum* exposure alters the functional properties of breast cancer cell *in vitro*. (a) Graph shows qPCR results of *F. nucleatum* detection in MCF7 cells passaged four-times after 72-hour co-culturing with *F. nucleatum* (FN27236 or FN146CP) and subsequent washing. **(b, c)** Trypan blue dye-exclusion assay showing

the number of viable MCF7 **(b)** and HCC1806 **(c)** cells 72 hours post-seeding. **(d, e)** Representative images of colony formation assay of breast cancer cells co-cultured with FN27236, 7-days post seeding. **(f)** Representative images showing the wound-healing assay of MCF7 cells passaged four-times after 72-hour co-culturing with *F. nucleatum* (FN27236 or FN146CP) and subsequent washing. **(g, h)** Representative images from mammosphere formation assay of MCF7 and HCC1806 cells exposed to *F. nucleatum* FN27236 with corresponding quantification. **(i)** Representative images showing matrigel-invasion and transwell-migration of HCC1937 cells exposed to *F. nucleatum* FN27236. **(j)** Representative immunocytochemistry images showing breast epithelial cells stained with PNA exhibiting cell surface abundance of Gal-GalNAc sugar residue. DAPI is used to stain the nuclei.

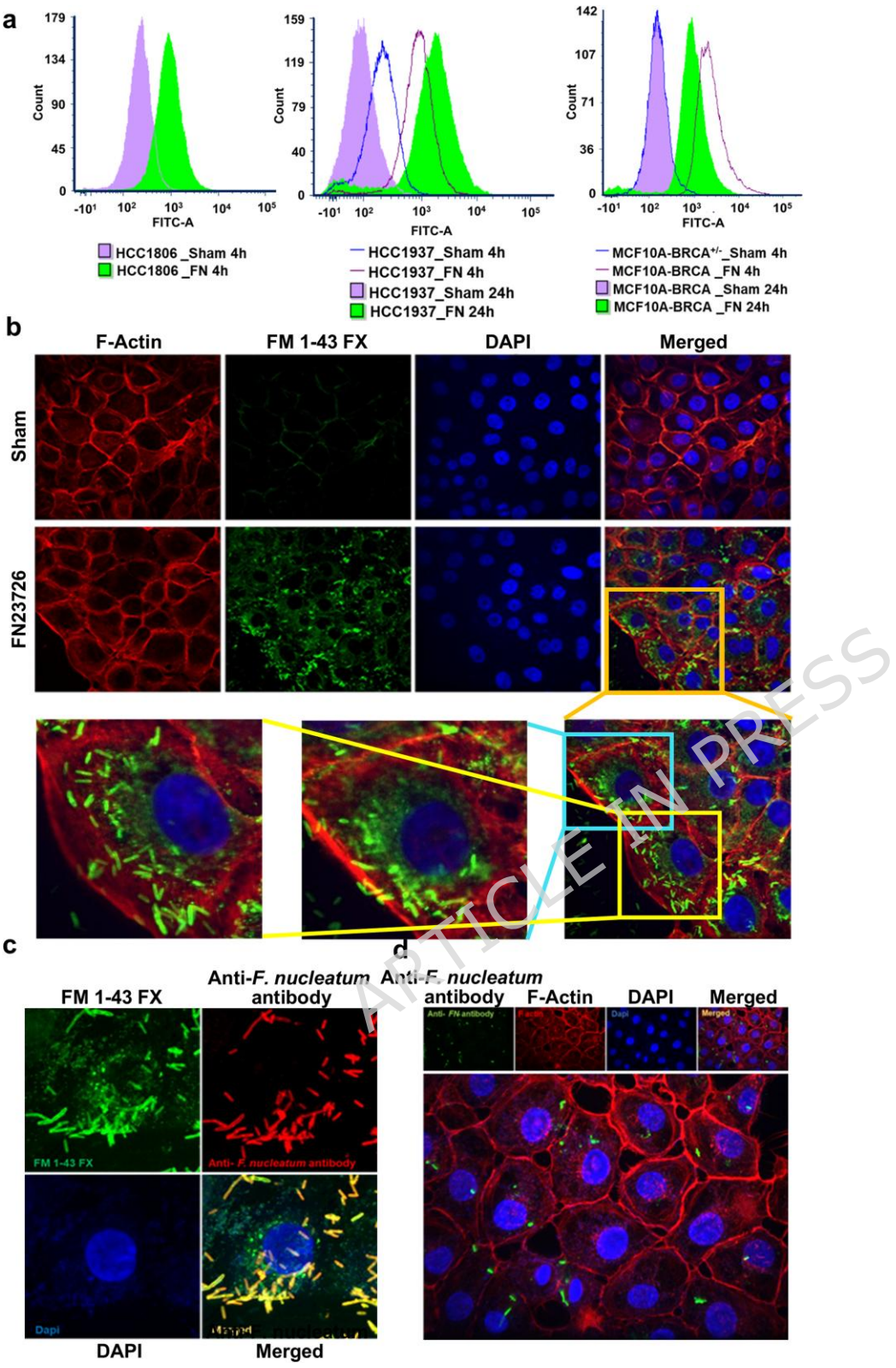

Figure 6. Cellular uptake and intracellular survival of *F. nucleatum*. (a) Graphs present flow cytometry results showing intracellular *F. nucleatum* after 4 h and 24 h of co-culturing with HCC1806, HCC1937 and MCF10A-BRCA+/- cells. **(b)** Representative photomicrographs showing the uptake of FM 1-43 FX tagged *F.*

nucleatum in MCF10A-BRCA+/- cells. DAPI is used to stain the nuclei. Phalloidin (red) is utilized to stain actin filaments. **(c)** Representative photomicrographs showing the FM 1-43 FX tagged *F. nucleatum* co-cultured with MCF10A-BRCA+/- followed by immunostaining with anti- *F. nucleatum* antibody without membrane permeabilization. **(d)** Representative photomicrographs showing the intracellular survival of FM 1-43 FX tagged *F. nucleatum* in MCF10A-BRCA+/- cells after 2 passages.

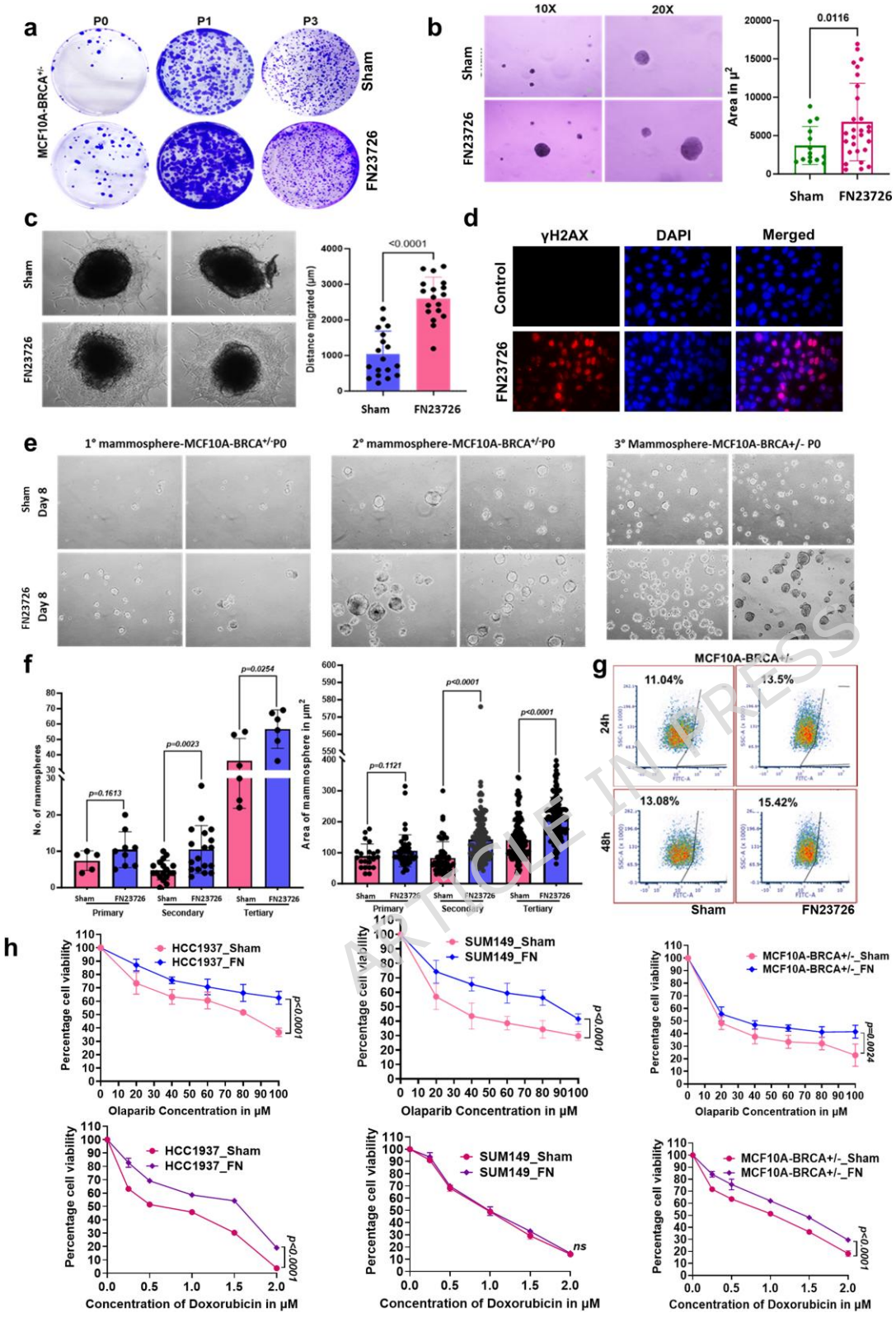

Figure 7. MCF10A-BRCA+/- cells exhibit altered functional properties as well as reduced olaparib and doxorubicin responsiveness upon *F. nucleatum* exposure. (a) Representative images show anchorage-dependent colony formation of MCF10A-BRCA+/- cells exposed to *F. nucleatum* followed by one (P1) or three

(P3) passages. **(b)** Representative images show anchorage-independent colony formation (soft-agar colony-formation) of MCF10A-BRCA+/- cells exposed to *F. nucleatum*. Bar graph shows quantitative representation of the area of soft-agar colonies. N=3, Between group comparison by student's t test. **(c)** Representative images show spheroid-migration of MCF10A-BRCA+/- cells exposed to *F. nucleatum* FN27236. Bar graph shows quantitative representation of distance migrated by the cells. N=3, Between group comparison by student's t test. **(d)** Representative immunocytochemistry images showing MCF10A-BRCA+/- cells exposed to *F. nucleatum* FN27236 and stained with γH2AX antibodies, as indicated. DAPI is used to stain the nuclei. **(e)** Representative images of mammospheres (primary, secondary and tertiary) formed by MCF10A-BRCA+/- cells exposed to *F. nucleatum* FN27236. **(f)** Bar graphs show the number and area of mammospheres formed in each group. N=3, Between group comparison by student's t test. **(g)** Representative data for ALDH1 activity in MCF10A-BRCA+/- cells exposed to *F. nucleatum* FN27236. **(h)** Dose response curves showing viability of MCF10A-BRCA+/-, HCC1937 and SUM149 cells exposed to *F. nucleatum* FN27236 (P2), in response to varying concentrations of Olaparib and Doxorubicin. Viability of cells were determined by MTT assay at 48 hours in two independent experiments with 4 replicates per group in each experiment (N=8). Dose response curves of Sham vs FN-cocultured cells was compared using 2 way ANOVA.

Declarations

Ethics approval and consent to participate: All animal studies were conducted in accordance with the guidelines of Johns Hopkins University Animal Care and Use Committee and are reviewed by Johns Hopkins ACUC. No Human data are reported here.

Consent for Publication: NA.

Availability of data and materials: The datasets used and/or analyzed during the current study and materials are available from the corresponding author on reasonable request.

Competing interests: The authors declare that they have no competing interests.

Funding: This work was supported by the Breast Cancer Research Foundation (BCRF) 90047965, CDMRP DOD BCRP (BC191572, BC210668) and The Fetting Fund for Cancer Prevention to Dipali Sharma; support from Bloomberg Philanthropies (BKI) to Cynthia L. Sears.

Author Contributions: SP carried out the animal experiments, in vitro experiments and wrote the first draft, DN participated in the functional assays, DV analyzed the RNA sequencing data, MY participated in the functional assays for bacteria infected cells, AY carried out the flow experiments, JQ participated in culturing bacteria and key discussions, KLG participated in animal experiments, CLS participated in the design of the study, DS designed and coordinated the study and helped to draft the manuscript. All authors read and approved the final manuscript.

Acknowledgements: We are grateful to Dr. Ben Park, Vanderbilt University, for mutant-MCF10A cell lines (MCF10A-BRCA+/-, p53 KO, p53-DKI, Kras and PTEN); Dr Daniel J. Slade, VerginiaTech, for *anti-F. nucleatum* antibody, Dr. Jessica Queen, Johns Hopkins Medicine for *F. nucleatum* strain FN146CP; Dr. Xinqun Wu and Dr. Shaoguang Wu for technical support.

REFERENCES

1. Brewer, H.R., et al., *Family history and risk of breast cancer: an analysis accounting for family structure.* Breast Cancer Res Treat, 2017. **165**(1): p. 193-200.
2. Zhang, Y., et al., *Analysis of Breast Cancer Family History, Estrogen Receptor Status, and Breast Cancer Outcomes in Sweden.* JAMA Netw Open, 2023. **6**(6): p. e2318053.

3. Effiong, M.E., et al., *Microbiome Dynamics in Breast Cancer: Mechanisms, Therapeutic Impacts and Research gaps.* Crit Rev Oncol Hematol, 2025: p. 104879.

4. Xuan, C., et al., *Microbial dysbiosis is associated with human breast cancer.* PloS one, 2014. **9**(1): p. e83744.

5. Urbaniak, C., et al., *The Microbiota of Breast Tissue and Its Association with Breast Cancer.* Applied and environmental microbiology, 2016. **82**(16): p. 5039-48.

6. Hieken, T.J., et al., *The Microbiome of Aseptically Collected Human Breast Tissue in Benign and Malignant Disease.* Scientific reports, 2016. **6**: p. 30751.

7. Chan, A.A., et al., *Characterization of the microbiome of nipple aspirate fluid of breast cancer survivors.* Scientific reports, 2016. **6**: p. 28061.

8. Costantini, L., et al., *Characterization of human breast tissue microbiota from core needle biopsies through the analysis of multi hypervariable 16S-rRNA gene regions.* Scientific reports, 2018. **8**(1): p. 16893.

9. Meng, S., et al., *Study of Microbiomes in Aseptically Collected Samples of Human Breast Tissue Using Needle Biopsy and the Potential Role of in situ Tissue Microbiomes for Promoting Malignancy.* Frontiers in oncology, 2018. **8**: p. 318.

10. Goedert, J.J., et al., *Investigation of the association between the fecal microbiota and breast cancer in postmenopausal women: a population-based case-control pilot study.* Journal of the National Cancer Institute, 2015. **107**(8).

11. Zhu, J., et al., *Breast cancer in postmenopausal women is associated with an altered gut metagenome.* Microbiome, 2018. **6**(1): p. 136.

12. Parida, S., et al., *A Procarcinogenic Colon Microbe Promotes Breast Tumorigenesis and Metastatic Progression and Concomitantly Activates Notch and β-Catenin Axes.* Cancer Discovery, 2021. **11**(5): p. 1138-1157.

13. Parida, S., et al., *Gut colonization with an obesity-associated enteropathogenic microbe modulates the premetastatic niches to promote breast cancer lung and liver metastasis.* Front Immunol, 2023. **14**: p. 1194931.

14. Akase, T., et al., *Association of Fusobacterium nucleatum in human saliva with periodontal status and composition of the salivary microbiome including periodontopathogens.* Microbiol Spectr, 2024. **12**(12): p. e0085524.

15. Freudenheim, J.L., et al., *Periodontal Disease and Breast Cancer: Prospective Cohort Study of Postmenopausal Women.* Cancer Epidemiology, Biomarkers & Prevention, 2016. **25**(1): p. 43-50.

16. Nwizu, N.N., et al., *Periodontal Disease and Incident Cancer Risk among Postmenopausal Women: Results from the Women's Health Initiative Observational Cohort.* Cancer Epidemiol Biomarkers Prev, 2017. **26**(8): p. 1255-1265.

17. Dizdar, O., et al., *Increased cancer risk in patients with periodontitis.* Current Medical Research and Opinion, 2017. **33**(12): p. 2195-2200.

18. Sfreddo, C.S., et al., *Periodontitis and breast cancer: A case-control study.* Community Dent Oral Epidemiol, 2017. **45**(6): p. 545-551.

19. Akbari, E., J.B. Epstein, and F. Samim, *Unveiling the Hidden Links: Periodontal Disease, Fusobacterium Nucleatum, and Cancers.* Curr Oncol Rep, 2024. **26**(11): p. 1388-1397.

20. Rubinstein, M.R., et al., *Fusobacterium nucleatum promotes colorectal cancer by inducing Wnt/β-catenin modulator Annexin A1.* EMBO Rep, 2019. **20**(4).

21. Tang, B., et al., *MicroRNA-31 induced by Fusobacterium nucleatum infection promotes colorectal cancer tumorigenesis.* iScience, 2023. **26**(5): p. 106770.

22. Xu, Q., et al., *Fusobacterium nucleatum induces excess methyltransferase-like 3-mediated microRNA-4717-3p maturation to promote colorectal cancer cell proliferation.* Cancer Sci, 2022. **113**(11): p. 3787-3800.

23. Li, B., et al., *Fusobacterium nucleatum induces oxaliplatin resistance by inhibiting ferroptosis through E-cadherin/β-catenin/GPX4 axis in colorectal cancer.* Free Radic Biol Med, 2024. **220**: p. 125-138.

24. Martin-Gallausiaux, C., et al., *Fusobacterium nucleatum promotes inflammatory and anti-apoptotic responses in colorectal cancer cells via ADP-heptose release and ALPK1/TIFA axis activation.* Gut Microbes, 2024. **16**(1): p. 2295384.

25. Wang, N., et al., *Fusobacterium nucleatum induces chemoresistance in colorectal cancer by inhibiting pyroptosis via the Hippo pathway.* Gut Microbes, 2024. **16**(1): p. 2333790.

26. Udayasuryan, B., et al., *Fusobacterium nucleatum induces proliferation and migration in pancreatic cancer cells through host autocrine and paracrine signaling.* Sci Signal, 2022. **15**(756): p. eabn4948.

27. Hayashi, M., et al., *Intratumor Fusobacterium nucleatum promotes the progression of pancreatic cancer via the CXCL1-CXCR2 axis.* Cancer Sci, 2023. **114**(9): p. 3666-3678.

28. Sun, J., et al., *F. nucleatum facilitates oral squamous cell carcinoma progression via GLUT1-driven lactate production.* EBioMedicine, 2023. **88**: p. 104444.

29. Li, Z., et al., *F. Nucleatum enhances oral squamous cell carcinoma proliferation via E-cadherin/β-Catenin pathway.* BMC Oral Health, 2024. **24**(1): p. 518.

30. Da, J., et al., *Fusobacterium nucleatum Promotes Cisplatin-Resistance and Migration of Oral Squamous Carcinoma Cells by Up-Regulating Wnt5a-Mediated NFATc3 Expression.* Tohoku J Exp Med, 2021. **253**(4): p. 249-259.

31. Nomoto, D., et al., *Fusobacterium nucleatum promotes esophageal squamous cell carcinoma progression via the NOD1/RIPK2/NF-κB pathway.* Cancer Lett, 2022. **530**: p. 59-67.

32. Yáñez, L., et al., *Co-Culture of P. gingivalis and F. nucleatum Synergistically Elevates IL-6 Expression via TLR4 Signaling in Oral Keratinocytes.* Int J Mol Sci, 2024. **25**(7).

33. Geng, F., et al., *Fusobacterium nucleatum Caused DNA Damage and Promoted Cell Proliferation by the Ku70/p53 Pathway in Oral Cancer Cells.* DNA Cell Biol, 2020. **39**(1): p. 144-151.

34. Zhang, S., et al., *Fusobacterium nucleatum promotes epithelial-mesenchymal transiton through regulation of the lncRNA MIR4435-2HG/miR-296-5p/Akt2/SNAI1 signaling pathway.* Febs j, 2020. **287**(18): p. 4032-4047.

35. Baba, Y., et al., *Relationship between gut microbiome Fusobacterium nucleatum and LINE-1 methylation level in esophageal cancer.* Esophagus, 2023. **20**(4): p. 704-712.

36. Hsueh, C.Y., et al., *Fusobacterium nucleatum impairs DNA mismatch repair and stability in patients with squamous cell carcinoma of the head and neck.* Cancer, 2022. **128**(17): p. 3170-3184.

37. Yuan, X., et al., *Integrative methylome and transcriptome analysis reveals epigenetic regulation of Fusobacterium nucleatum in laryngeal cancer.* Microb Genom, 2024. **10**(3).

38. Chen, Z., et al., *The Intersection between Oral Microbiota, Host Gene Methylation and Patient Outcomes in Head and Neck Squamous Cell Carcinoma.* Cancers (Basel), 2020. **12**(11).

39. Yamamura, K., et al., *Intratumoral Fusobacterium Nucleatum Levels Predict Therapeutic Response to Neoadjuvant Chemotherapy in Esophageal Squamous Cell Carcinoma.* Clin Cancer Res, 2019. **25**(20): p. 6170-6179.

40. Zhang, N., et al., *Clinical Significance of Fusobacterium nucleatum Infection and Regulatory T Cell Enrichment in Esophageal Squamous Cell Carcinoma.* Pathol Oncol Res, 2021. **27**: p. 1609846.

41. Li, Z., et al., *Fusobacterium nucleatum predicts a high risk of metastasis for esophageal squamous cell carcinoma.* BMC Microbiol, 2021. **21**(1): p. 301.

42. Guo, X., K. Yu, and R. Huang, *The ways Fusobacterium nucleatum translocate to breast tissue and contribute to breast cancer development.* Mol Oral Microbiol, 2024. **39**(1): p. 1-11.

43. Parhi, L., et al., *Breast cancer colonization by Fusobacterium nucleatum accelerates tumor growth and metastatic progression.* Nat Commun, 2020. **11**(1): p. 3259.

44. Guo, J., et al., *Fusobacterium nucleatum promotes PD-L1 expression in cancer cells to evade CD8(+) T cell killing in breast cancer.* Hum Immunol, 2024. **85**(6): p. 111168.

45. Li, G., et al., *Fusobacterium nucleatum-derived small extracellular vesicles facilitate tumor growth and metastasis via TLR4 in breast cancer.* BMC Cancer, 2023. **23**(1): p. 473.

46. Hieken, T.J., et al., *The Microbiome of Aseptically Collected Human Breast Tissue in Benign and Malignant Disease.* Sci Rep, 2016. **6**: p. 30751.

47. Yin, H., et al., *Fusobacterium nucleatum promotes liver metastasis in colorectal cancer by regulating the hepatic immune niche and altering gut microbiota.* Aging (Albany NY), 2022. **14**(4): p. 1941-1958.

48. Hong, J., et al., *F. nucleatum targets lncRNA ENO1-IT1 to promote glycolysis and oncogenesis in colorectal cancer.* Gut, 2021. **70**(11): p. 2123-2137.

49. Parmar, A., et al., *Harnessing the oral-systemic axis: A novel frontier in cancer management.* Med Oncol, 2025. **42**(8): p. 348.

50. Huang, R. and P.K. Zhou, *DNA damage repair: historical perspectives, mechanistic pathways and clinical translation for targeted cancer therapy.* Signal Transduct Target Ther, 2021. **6**(1): p. 254.

51. Obst, B., et al., *Helicobacter pylori causes DNA damage in gastric epithelial cells.* Carcinogenesis, 2000. **21**(6): p. 1111-5.

52. Rai, P., et al., *Pneumococcal Pneumolysin Induces DNA Damage and Cell Cycle Arrest.* Sci Rep, 2016. **6**: p. 22972.

53. Shi, Y., et al., *Helicobacter pylori-Induced DNA Damage Is a Potential Driver for Human Gastric Cancer AGS Cells.* DNA Cell Biol, 2019. **38**(3): p. 272-280.

54. Xu, W., et al., *Elucidating the genotoxicity of Fusobacterium nucleatum-secreted mutagens in colorectal cancer carcinogenesis.* Gut Pathog, 2024. **16**(1): p. 50.

55. Zhang, J.W., et al., *Fusobacterium nucleatum promotes esophageal squamous cell carcinoma progression and chemoresistance by enhancing the secretion of chemotherapy-induced senescence-associated secretory phenotype via activation of DNA damage response pathway.* Gut Microbes, 2023. **15**(1): p. 2197836.

56. Collins, P.L., et al., *DNA double-strand breaks induce H2Ax phosphorylation domains in a contact-dependent manner.* Nature communications, 2020. **11**(1): p. 3158.

57. Li, X. and W.-D. Heyer, *Homologous recombination in DNA repair and DNA damage tolerance.* Cell research, 2008. **18**(1): p. 99-113.

58. Stephens, P.J., et al., *The landscape of cancer genes and mutational processes in breast cancer.* Nature, 2012. **486**(7403): p. 400-4.

59. Inagaki-Kawata, Y., et al., *Genetic and clinical landscape of breast cancers with germline BRCA1/2 variants.* Commun Biol, 2020. **3**(1): p. 578.

60. Parhi, L., et al., *Placental colonization by Fusobacterium nucleatum is mediated by binding of the Fap2 lectin to placentally displayed Gal-GalNAc.* Cell Rep, 2022. **38**(12): p. 110537.

61. Abed, J., et al., *Tumor Targeting by Fusobacterium nucleatum: A Pilot Study and Future Perspectives.* Front Cell Infect Microbiol, 2017. **7**: p. 295.

62. Li, R., J. Shen, and Y. Xu, *Fusobacterium nucleatum and Colorectal Cancer.* Infect Drug Resist, 2022. **15**: p. 1115-1120.

63. Andrikopoulou, A., et al., *The Mutational Landscape of Early-Onset Breast Cancer: A Next-Generation Sequencing Analysis.* Front Oncol, 2021. **11**: p. 797505.

64. Elstrodt, F., et al., *BRCA1 mutation analysis of 41 human breast cancer cell lines reveals three new deleterious mutants.* Cancer Res, 2006. **66**(1): p. 41-5.

65. Urbaniak, C., et al., *Microbiota of human breast tissue.* Applied and environmental microbiology, 2014. **80**(10): p. 3007-14.

66. Wang, H., et al., *Breast tissue, oral and urinary microbiomes in breast cancer.* Oncotarget, 2017. **8**(50): p. 88122-88138.

67. Fu, A., et al., *Tumor-resident intracellular microbiota promotes metastatic colonization in breast cancer.* Cell, 2022. **185**(8): p. 1356-1372.e26.

68. Parida, S. and D. Sharma, *The Microbiome-Estrogen Connection and Breast Cancer Risk.* Cells, 2019. **8**(12).

69. Parida, S. and D. Sharma, *Microbial Alterations and Risk Factors of Breast Cancer: Connections and Mechanistic Insights.* Cells, 2020. **9**(5).

70. Parida, S. and D. Sharma, *The Microbiome and Cancer: Creating Friendly Neighborhoods and Removing the Foes Within.* Cancer Research, 2021. **81**(4): p. 790-800.

71. Xu, C., et al., *Fusobacterium nucleatum promotes colorectal cancer metastasis through miR-1322/CCL20 axis and M2 polarization.* Gut Microbes, 2021. **13**(1): p. 1980347.

72. Zhang, Y., et al., *Fusobacterium nucleatum promotes colorectal cancer cells adhesion to endothelial cells and facilitates extravasation and metastasis by inducing ALPK1/NF-κB/ICAM1 axis.* Gut Microbes, 2022. **14**(1): p. 2038852.

73. Chen, S., et al., *Fusobacterium nucleatum reduces METTL3-mediated m(6)A modification and contributes to colorectal cancer metastasis.* Nat Commun, 2022. **13**(1): p. 1248.

74. Casasanta, M.A., et al., *Fusobacterium nucleatum host-cell binding and invasion induces IL-8 and CXCL1 secretion that drives colorectal cancer cell migration.* Sci Signal, 2020. **13**(641).

75. Ou, S., et al., *Fusobacterium nucleatum upregulates MMP7 to promote metastasis-related characteristics of colorectal cancer cell via activating MAPK(JNK)-AP1 axis.* J Transl Med, 2023. **21**(1): p. 704.

76. Yue, X., et al., *DNA-PKcs: A Multi-Faceted Player in DNA Damage Response.* Front Genet, 2020. **11**: p. 607428.

77. Love, M.I., W. Huber, and S. Anders, *Moderated estimation of fold change and dispersion for RNA-seq data with DESeq2.* Genome Biol, 2014. **15**(12): p. 550.

78. Ge, S.X., E.W. Son, and R. Yao, *iDEP: an integrated web application for differential expression and pathway analysis of RNA-Seq data.* BMC Bioinformatics, 2018. **19**(1): p. 534.

79. Subramanian, A., et al., *Gene set enrichment analysis: a knowledge-based approach for interpreting genome-wide expression profiles.* Proc Natl Acad Sci U S A, 2005. **102**(43): p. 15545-50.

80. Muniraj, N., et al., *Withaferin A inhibits lysosomal activity to block autophagic flux and induces apoptosis via energetic impairment in breast cancer cells.* Carcinogenesis, 2019. **40**(9): p. 1110-1120.

81. Xie, B., et al., *Benzyl Isothiocyanate potentiates p53 signaling and antitumor effects against breast cancer through activation of p53-LKB1 and p73-LKB1 axes.* Sci Rep, 2017. **7**: p. 40070.